PHYSICAL REVIEW B VOLUME 39, NUMBER 3 15 JANUARY 1989-II

Dimer–adatom–stacking-fault (DAS) and non-DAS (111) semiconductor surfaces: A comparison of Ge(111)-$c(2\times8)$ to Si(111)-(2×2), -(5×5), -(7×7), and -(9×9) with scanning tunneling microscopy

R. S. Becker, B. S. Swartzentruber*, J. S. Vickers, and T. Klitsner
AT&T Bell Laboratories, Murray Hill, New Jersey 07974-2070

(Received 22 March 1988; revised manuscript received 12 July 1988)

We have examined the Ge(111)-$c(2\times8)$ and related surfaces in detail with the scanning tunneling microscope. A comparison of tunneling images in both filled and empty states for the Ge(111) surface with similar images for Si(111)-(5×5), -(7×7), and -(9×9) surfaces shows the surface structure to be inconsistent with recent models, such as the dimer chain proposed by Takayanagi and collaborators. Comparison with filled- or empty-state images for the laser-stabilized Si(111) surface shows that both this surface and the Ge(111)-$c(2\times8)$ are most consistent with a simple model of alternating rows of 2×2 and $c(4\times2)$ adatoms on T_4 sites on a 1×1 substrate. We find no evidence in the tunneling images of Ge(111)-$c(2\times8)$ to support the existence of a subsurface stacking fault. Electronic and geometric sources for the contrast in the tunneling images are considered and it is concluded that electronic structure forms the basis for the images of adatom-reconstructed semiconductor surfaces.

For the past 30 years the Si(111) surface's native reconstruction, the 7×7, has been the object of intense study by a full array of surface-physics techniques. Within the last few years consensus has been reached, based in part on new information gathered by both the scanning-tunneling-microscope (STM) and transmission-electron-diffraction studies, that a model proposed by Takayanagi and co-workers consisting of dimers, adatoms, and a partial subsurface stacking fault (the DAS model) best describes the equilibrium surface.[1] Inspection of this model shows that it can be trivially extended to any $(2n+1)\times(2n+1)$ size. Subsequent to the proposal of this model by Takayanagi, a smaller example of this structure, the 5×5, was discovered on the (111) surface of an alloy of germanium and silicon,[2] and verified with the tunneling microscope.[3] Further, photoemission[4] and core-level spectroscopy[5] carried out on another alloy, SnGe(111), where ~0.25 monolayer of Sn is deposited on Ge(111), indicate that the 7×7 reconstruction exhibited by that surface is very similar to that displayed by Si(111). Indeed, tunneling images of this surface appear to be nearly identical with those for Si(111).[6]

Despite the success enjoyed in determining the nature of the Si(111) surface, the equilibrium room-temperature phase displayed by Ge(111), the $c(2\times8)$, has remained somewhat mysterious. Early investigators determined from an analysis of the "missing" beams in low-energy electron diffraction (LEED) studies on sputtered and annealed Ge(111) that the unit mesh was not threefold symmetric, but that the apparent threefold symmetry of the diffraction pattern was due to the presence of multiple twinned 2×8 domains on the surface,[7] rather than an 8×8 structure. Later, it was pointed out that the LEED patterns are better explained by twinned domains of $c(2\times8)$ symmetry.[8] However, studies of the surface-electronic structure using angle-resolved ultraviolet photoemission spectroscopy (ARUPS) have shown the Ge(111) and Si(111) surface bands to be similar, both indicating elements of structures with a two periodicity.[4,9–12] More recently, tunneling-microscope observations of the Ge(111) surface have shown a multiplicity of protrusion-based structures,[13] similar in short-range order to the protrusions on each half of the Si(111)-(7×7) mesh noted in STM studies on that system.[14–17] Domains of 2×2 and $c(4\times2)$ were observed, and the $c(2\times8)$ unit mesh was demonstrated to consist of a coherent stacking of the 2×2 and $c(4\times2)$ subunits, alternating row by row. The tunneling images in that work were unable to discern the nature of the protrusions, their positions with respect to the underlying lattice, or the nature of the underlying structure.

In this work we present a comprehensive study with the STM of the nature of the Ge(111)-$c(2\times8)$ reconstruction. To accomplish this, detailed dual polarity images of this surface, acquired tunneling at bias voltages that access empty states above the Fermi energy E_F, and filled states located just below E_F are compared with similar images for three members of the dimer–adatom–stacking-fault (DAS) family, Si(111)-(5×5), (7×7), and (9×9). Further comparisons are made with dual polarity tunneling images acquired on the laser-stabilized Si(111)-(2×2) surface, whose reconstruction is demonstrated to be very similar to the Ge(111) surface. The tunneling images for the Ge(111) and laser-stabilized Si(111) surfaces are shown to be most consistent with a simple model consisting of adatoms loosely populating a 1×1 substrate. We interpret the tunneling images for these adatom reconstructed surfaces principally in terms of imaging occupied and unoccupied dangling bonds, and demonstrate that the apparent heights in the data are completely dominated by electronic rather than geometric sources of contrast. Tunnel-junction I-V

characteristics for all of the surface reconstructions are presented and shown to be generally similar, but possessing significant differences which are related to the substrate reconstruction in the DAS structures.

EXPERIMENT

The tunneling images and junction *I*-*V* characteristics reported in this work were acquired with two room-temperature ultrahigh-vacuum (UHV) tunneling microscopes. Details of one of them, a three-axis piezoelectric stick design, have been reported elsewhere.[13] The other microscope consists of a cylindrical piezoelectric transducer divided into four equal sectors.[18] The sectors are driven differentially to provide motion in x and y (parallel to the sample surface), and driven synchronously to provide motion in z (perpendicular to the sample surface). Application of high voltage (-150 to $+150$ V) gives a lateral range of 2 μm with a vertical range of 6000 Å. Measured stability, obtained from the noise characteristics of the high-voltage drivers and determined from tunneling images of Si(111), is 0.2 Å laterally and 0.01–0.05 Å vertically. Both microscopes are housed in UHV chambers (base pressure 5×10^{-11} Torr) equipped with facilities for ion sputtering (Ar^+ or Ne^+), thermal annealing, laser annealing, and a combined LEED-Auger apparatus for sample surface-order and cleanliness characterization. The tunneling tips are made from polycrystalline tungsten wire, 0.020 in. in diameter, electrochemically hydroxide etched to a macroscopic radius of curvature of ~1000 Å, and cleaned *in situ* by field emission at several μA.

The samples were cut from 0.020-in.-thick Syton polished wafers of Si and Ge. The Si wafers were *n*-type (As

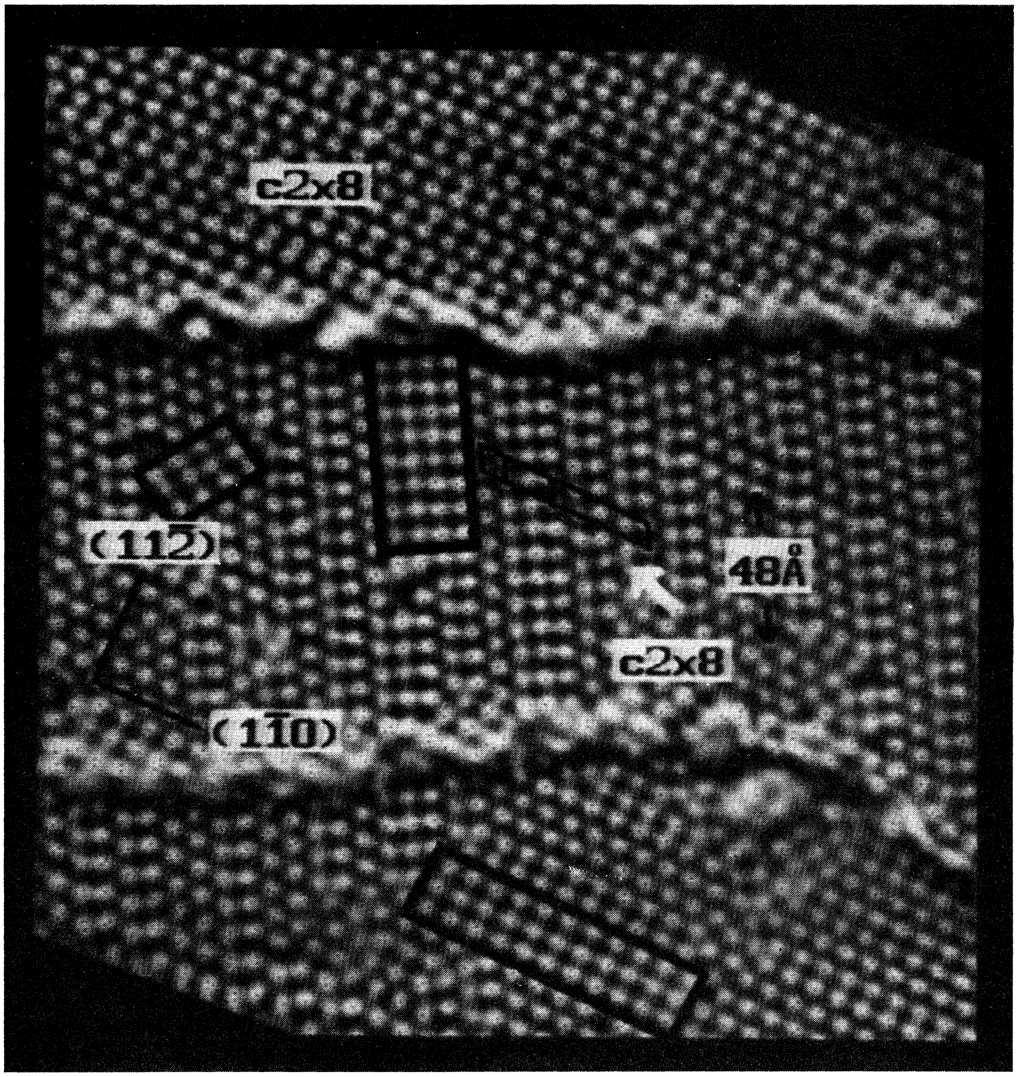

FIG. 1. Tunneling image of the Ge(111) surface. The grey scale rendering is keyed on curvature, reflecting local height, with a dynamic range of ~1 Å. The principal crystallographic directions are indicated, as are local regions of 2×2, $c(4\times2)$, and $c(2\times8)$ symmetry. Two atomic steps are seen running across the image, which is approximately 260 by 300 Å. This image was acquired tunneling into empty sample states at a bias voltage of 1.0 V at a tunneling current of 40 pA.

and Sb doped, 0.01–0.002 Ω cm), while the Ge samples were both *n*- and *p*-type (Sb doped, 0.1 Ω cm; Ga doped, 0.002 Ω cm). The sample surfaces were prepared using a variety of techniques. The Si samples were generally chemically etched using the Shiraki method,[19] with the protective oxide removed in UHV by annealing at 900–950 °C for 5–10 min, followed by cooling at rates ranging from 1 °C/s to quenching at ∼100 °C/s. These procedures result in large terraces of 7×7 reconstruction, 500–2000 Å in extent, with many antiphase boundaries detected on the rapidly quenched samples. Examples of 5×5 and 9×9 reconstructions were created by either sputtering with 1.0-kV Ar^+ or Ne^+ ions, or laser annealing the Shiraki etched surface, then reannealing at 550 °C for 10–14 h. Si surfaces prepared by these latter procedures consist of approximately 20% 5×5 and 80% 7×7.[20] Careful surveying with the STM revealed small areas, no larger than two unit meshes, of 9×9 symmetry. The Ge(111) surfaces were prepared by sputtering (Ar^+,Ne^+ at 1.0 kV) followed by thermal annealing. Several annealing procedures were used during the coarse of the work on the Ge(111) surfaces. Annealing at 800–850 °C for 5–10 min followed by cooling at 1 °C/s until the sample reached 500 °C, then quenching resulted in domains of $c(2\times8)$, 2×2, and $c(4\times2)$ with typical terrace sizes of 500–1000 Å in extent. Ge surfaces prepared in this manner tended to display "mounds" of unidentified debris covering ∼10% of the sample surface. Alternatively, the Ge(111) samples were annealed at sample temperatures of 550 and 640 °C for 10–12 h. This procedure yielded stepped terraces 100–300 Å in extent (due to the slightly offcut nature of the wafer) with regions of $c(2\times8)$ intermixed with regions of 2×2 and $c(4\times2)$. In contrast to the high-temperature–short-time anneals, the long-period anneal showed no debris mounds. Figure 1 shows a tunneling image of a typical Ge(111)-$c(2\times8)$ surface prepared by these techniques. In the figure, regions of local 2×2, $c(4\times2)$, and $c(2\times8)$ symmetry are seen along with two double-layer single atomic steps. The thin black lines depict 2×2, $c(4\times2)$, and $c(2\times8)$ unit meshes, while the heavy black lines delineate three twinned domains of $c(4\times2)$. This picture is similar to, but of greater extent than, that reported in an earlier STM study on the Ge(111)-$c(2\times8)$ surface.[13] This image was acquired tunneling from the tip into empty sample states at a bias of 1.0 V and a current of 40 pA. We call attention to the fact that the surface is covered by protrusions with an apparent height of ∼1.0 Å, remarkably similar in appearance to the protrusions reported on the Si(111)-(7×7) surfaces imaged with the STM.[14–17] In contrast to the tunneling images of the Si(111)-(7×7) surface which show remarkable order over distance scales as large as 1000 Å, the Ge(111) surface usually displays small $c(2\times8)$ domains only 200 Å in extent, with many regions of 2×2 and $c(4\times2)$ symmetry interspersed with the $c(2\times8)$. This fundamental difference between the Si(111) and Ge(111) surfaces, so obviously evident in the tunneling images, is undoubtedly dictated by a profound difference in subsurface atomic arrangement. This subsurface reconstruction of Ge(111) is the principal focus of the remainder of this work. However, in order to understand the details of the Ge(111) tunneling images, a review of the principles of STM image formation, the details of Si(111) tunneling images for DAS and non-DAS Si surfaces, and their relationship to the DAS model for the Si(111)-($[2n+1]\times[2n+1]$) reconstruction is required.

DATA AND METHODS

The analysis of surface geometry with tunneling images naturally brings into question the interpretation of the source of the symmetry and apparent heights displayed in the images. When the microscope operates in the constant current mode (as it is in all images shown in this work), the feedback electronics servos the scanning tip in and out in order to maintain a preset, fixed tunneling current. These changes in the z position of the tip (feedback error) are interpreted as heights and form the basis for the tunneling images. The origin of the changes in tunneling probability which cause the tip to be servoed arise from at least two sources: a change in the physical height of the surface atoms (such as a step), or a change in either the occupied or unoccupied electron state density of the sample at or below the tunneling bias voltage (such as a dangling bond). In the case of a metal, where a partially filled band exists at the Fermi level and the tunneling bias voltage is much less than the tunneling barrier height, the elegant theory of Tersoff and Hamann predicts the contours of constant tunneling probability to closely reflect the contours of constant charge density at the Fermi level.[21] Since metallic bonding is not strongly directional, these contours are simply interpreted as the geometric positions of the surface atoms. *I*-*V* characteristics of the tunnel junction acquired on clean metal surfaces typically display no strong spatially varying features, indicating the lack of spatial variation in electronic characteristics.[22] The situation for tunneling images taken of semiconductor surfaces is considerably more complex, due to both the presence of a bulk and/or surface band gap requiring larger (∼1.0 V) junction bias voltages, and to the close coupling between spatial variations in geometric and electronic structure. Early work on Si(111)-(7×7) and Si(001)-(2×1) (Refs. 16, 23, and 24) utilizing the method of tunnel *current imaging* indicated that the spatial distribution of surface electronic states may be determined with the STM. However, later work by Feenstra and co-workers[25] showed that the spatial variations in tunnel *current images* at a given bias condition can be dominated by the changes in the tunneling barrier due to the local sample geometry, and could lead to erroneous conclusions. Further work by this group on Si(111)-(2×1) (Ref. 26) and GaAs(110) (Ref. 27) demonstrated that it is possible to glean information relating to the separation of geometric and electronic characteristics through a detailed comparison of *tunneling images* (feedback error) simultaneously acquired tunneling into empty sample states and out of filled sample states near the edges of the surface energy gap. These image pairs may be acquired simultaneously by gating the feedback loop and junction bias polarity, taking one image scanning "forward" (from left to right) and the other while scanning "back" (from right to left). Hysterisis correction (if needed) arising from the scanning element may be measured with a control set of images taken at identical bias and polarity conditions in both directions.

Figures 2(a)–2(c) are such a set of dual polarity tunneling images of a Si(111)-(7×7) surface. In the figure, blue represents an image acquired tunneling from the tip into empty sample states at a bias of +1.0 V, while orange represents the image acquired when tunneling out of filled sample states into empty tip states at a bias voltage of −1.0 V. Both images were taken at a demanded tunneling current of 1.0 nA. In Fig. 2(b) the images in Fig. 2(a) and 2(c) are overlaid to illustrate the superposition of occupied and unoccupied state signals. The color saturation in these images is keyed on apparent height, with a range of 1.5 Å used in Fig. 2. The crystallographic orientation is as indicated, as are the faulted and unfaulted halves of the unit mesh. Several features characteristic of 7×7 tunneling images are immediately seen. First, the faulted half of the unit mesh's six protrusions appears to be higher than the corresponding protrusions in the unfaulted half of the mesh in the filled-state image, an effect reported previously in Refs. 14 and 16. Second, the entire unfaulted side of the mesh appears ∼0.1 Å higher in the corresponding empty-state image, as reported in Ref. 15. Third, significant signal is detected at intermediate positions (X) in the filled-state image between corner protrusions (C) and middle protrusions (M) on both sides of the unit mesh. Fourth, the protrusions at the corners of both halves of the unit mesh appear higher than the middle protrusions. When the occupied-(orange) and unoccupied- (blue) state images are combined in Fig. 2(b), we see that the protrusions in both filled- and empty-state images coincide with the faulted mesh side appearing significantly whiter than the unfaulted mesh side. We see no superposition of apparent height signal in the intermediate positions between corner and middle protrusions. In neither image is there any signal in the gaps between protrusions on the boundary between mesh halves.

We have found, by carefully studying the tunneling images acquired on Si(111)-(7×7) surfaces, that the above features are common to image pairs displaying good threefold symmetry *regardless of the detailed state of the tunneling tip.* The effects of the geometric and electronic structure of the tip on tunneling images has been addressed elsewhere,[17,28,29] while an exhaustive examination of the effects of the stabilization bias voltage on the measured I-V characteristics and current-difference images is contained in Ref. 17. In the latter work, it is concluded that the stabilization voltage set point has profound effects on both the magnitude and apparent spatial conformation of *current* images, while having a much smaller effect on the *feedback stabilization* tunneling images. In general, the electronic structure of the unoccupied states on *both* sides of the junction can significantly affect measured I-V characteristics, but has less effect on the features of tunneling images taken of unoccupied states just above the surface energy gap, and filled states just below the gap. This is due to the fact that when tunneling from the tip to the empty sample states, the tunneling barrier weights against *tip* states that are very far from the Fermi energy E_F, confining 90% of the tunnel current to within 0.5–1.0 eV of E_F of the tip, and the image reflects, for the most part, the spatial configuration of the unoccupied sample states. Conversely, when tunneling from the sample back to the tip, the tunneling barrier now weights against *sample* states that are very far from the sample E_F. In this case, changing the junction bias voltage V_b over a limited range (∼1.5 V) only weakly effects the apparent spatial conformation of the sample states, and primarily acts to reduce the height contrast by increasing the vacuum gap.[29] Since *tunneling images* (feedback error) are formed by integrating all the tunnel current from the source Fermi level down to the drain Fermi level, they are less susceptible to variations in tip electronic or geometric structure than the analogous current difference images, which derive their contrast from a small portion of the tunnel current.

One can understand the images in Fig. 2 by comparison to the generally accepted Takayanagi-Tanishino-Takahashi-Takahashi DAS model for the 7×7 reconstruction.[1] A ball-and-stick model of the DAS-(7×7) is shown in plan view in Fig. 3. Here, for comparison with the data in Fig. 2, the various atoms are colored to match the tunneling images, with adatoms in white, rest atoms with unsatisfied dangling bonds in red, faulted-half substrate backbond atoms in orange, unfaulted-half substrate backbond atoms in blue, and dimerized substrate atoms along wall boundaries in magenta. We see that the 12 protrusions in the unit mesh seen in both the occupied- and unoccupied-state images correspond to the adatoms in the DAS model. The excess of signal between the corner and middle adatom positions in the occupied-state image corresponds to the dangling bond on the rest atom located at this position in the mesh. Since no similar rest-atom dangling bonds are found on the dimer walls joining mesh halves, no signal is seen here. This interpretation of the tunneling images is similar to that given by Hamers *et al.* in their earlier work on the Si(111)-(7×7) surface.[16,23] Indeed, the authors of that work report that occasionally signal can be detected from the bottom of the corner holes in the unit mesh. They attribute this to the presence of a dangling bond similar to that for the rest atoms in the bottom of the corner depression, as required by the DAS model. We note that this interpretation is essentially a dangling-bond interpretation of the tunneling images, i.e., the STM images on semiconductors are composed almost entirely from the locations of filled and empty dangling bonds. Strong evidence for this comes from work by Feenstra *et al.* on GaAs(110),[27] where superposition of tunneling images acquired from occupied and unoccupied states showed the unoccupied states to correspond to the Ga surface atoms and the occupied states to the more electronegative As surface atoms. These investigators have extended this technique of dangling-bond imaging to an analysis of reconstructed steps on the cleaved Si(111) surface where the reconstruction is similar to the 2×1 π-bonded chain.[30] Here, they are able to clearly distinguish between competing models for the reconstruction of the step riser through a one-to-one mapping of unterminated dangling bonds to protrusions in the filled-state tunneling images. This dangling-bond analysis has also recently been applied by Wierenga *et al.* to a study of biatomic steps on vicinal Si(001),[31] where a rebonded geometry consisting of partial asymmetric dimers was shown to best describe the tunneling images instead of a π-bonded chain reconstruction of the biatomic step riser.

We have taken data on two related DAS structures, the 5×5 and 9×9 reconstructions occasionally found on the Si(111) surface. Comparison of these with the 7×7 images provides a good test of this simple dangling-bond interpretation as the size of the unit cell is shrunk down or enlarged. Figures 4(a) and 4(b) show such a comparison of the tunneling images for the Si(111)-(5×5) and -(9×9) superstructures, with the principal crystallographic directions indicated. In Fig. 4(a), a superposition of empty-(blue) and filled-(orange) state images for the 5×5 is displayed. Again, we have several features which reproduce independent of the tip structure. Due to the down scaling of the mesh size, there are six protrusions per 5×5 mesh as opposed to twelve in the 7×7 reconstruction. The three protrusions on the faulted half of the unit mesh appear higher than the corresponding protrusions on the unfaulted half in the filled-state images. In the filled-state image, signal is detected at the position between the protrusions in the center of both halves of the unit mesh, while it is not detected in the empty-state image. The tunneling images for the Si(111)-(9×9) in Fig. 4(b) show 20 protrusions per unit mesh. The common features of the 9×9 images are the same as those for the 7×7 with one addition: the center protrusion in both halves of the unit mesh is a small amount *lower* in the empty-state image,[32] and essentially *vanishes* in the corresponding filled-state image. This is evident in the superposition image of Fig. 4(b) where the center protrusions are seen to be strongly blue in comparison with the whiter color of surrounding protrusions.

Extending the interpretation of the 7×7 tunneling image to those of the 5×5 and 9×9, it is seen that the Takayanagi-Tanishiro-Takahashi-Takahashi DAS model can be scaled down to the 5×5 and up to the 9×9, accounting for the protrusions as adatoms on T_4 (closed) sites on the mesh halves, and the excess of filled-state signal between corner and middle protrusions as rest-atom dangling bonds. The absence of any such excess signal in the boundary regions adjoining mesh halves is simply explained by the dimerization into five- and eight-member rings eliminating dangling bonds. The difference in apparent height between the unit mesh halves for the DAS structures, most easily seen in both occupied- and unoccupied-state tunneling images for the 7×7 case where the faulted side is higher in filled-state images while the unfaulted side is higher in empty-state images, is due to the partial stacking fault which slightly alters the density and/or energy position of backbond states between the mesh halves. Since the adatom dangling bonds superimpose in both filled- and empty-state images, it is apparent that they occupy a partially filled surface band straddling E_F. This supports ultraviolet photoemission spectroscopy (UPS) work on Si(111) and SnGe(111) 7×7 (Refs. 4 and 33) reporting surface features with p_z characteristics that were attributed to dangling bonds at or close to E_F.

To understand the electronic structure which leads to this superposition of filled- and empty-state images, we consider a recent first-principles pseudopotential calculation by Northrup of the valence-band states present on a Si(111)-($\sqrt{3}\times\sqrt{3}$)-Si adatom geometry.[34] Northrup interprets the electronic structure of the Si(111)-(7×7) surface in terms of T_4 site adatom-induced states and rest-atom dangling-bond states. For the case of the $\sqrt{3}\times\sqrt{3}$ geometry, where there are no rest-atom dangling bonds, he finds a partially filled surface band lying at, and pinning, the Fermi level, and a deeper band at 1.5–2.0 eV below E_F corresponding to substrate dangling bonds coupling to p_x and p_y adatom orbitals. He concludes that the observed S_2 surface state at -0.8 V is due to a completely filled band arising from the rest-atom dangling bonds in the 2×2 adatom geometry found on the 7×7 mesh halves. Northrup further argues that the dangling-bond electrons found on the DAS surfaces can be taken as a group, first filling the lower-lying rest-atom band, then putting the remaining electrons into the surface band comprising the photoemission S_1 peak associated with the adatom dangling bonds. For the 5×5, 7×7, and 9×9 DAS geometries this results in a completely filled rest-atom band, and adatom bands that are 0.33, 0.25, and 0.20 occupied. This electron counting neglects the dangling bond in the deep corner hole, which can be included as a rest-atom dangling bond without significantly altering the S_1 band filling. This predicts that the adatoms should be imaged in the same positions both tunneling into empty sample states at the surface conduction band edge, and tunneling out of filled sample states at the surface valence-band edge, precisely as is shown in Figs. 2 and 4 for the Si(111) DAS structures.

Several additional details in the tunneling images for the Si(111) DAS surfaces merit comment. The data in Figs. 2 and 4 show a smooth progression from the 5×5 with one species of adatom [corner (C)], through the 7×7 with two species [corner (C) and middle (M)], to the 9×9 where there exist *three* adatom types: corner (C), middle (M), and interior (I). For the tunneling images acquired from filled sample states near E_F, the progression in decreasing apparent height is C, M, I. There is more filled-state density in the dangling-bond bands on the C adatoms, somewhat less (0.2 Å in height) on the M adatoms, and very little on the I adatom of the 9×9 which lies an additional 0.3 Å below the M adatoms in apparent height. This change in apparent height of 0.5 Å going from the C to the I adatom represents a change in tunneling probability of approximately a factor of 3. The interior (I) adatom on the 9×9 is on a T_4 site bounded by three rest-atom dangling bonds, the M adatoms are adjacent to two rest-atom dangling bonds, while the C adatoms are adjacent to one rest-atom dangling bond. Thus, there is a small amount of charge transfer from the C adatoms to the filled rest-atom band, somewhat more from the M adatoms to the rest atoms, and an almost complete transfer from the I adatom to the rest-atom band, accounting for the contrast seen in the images.

Additional information on the source of the contrast in the tunneling images can be obtained from high-

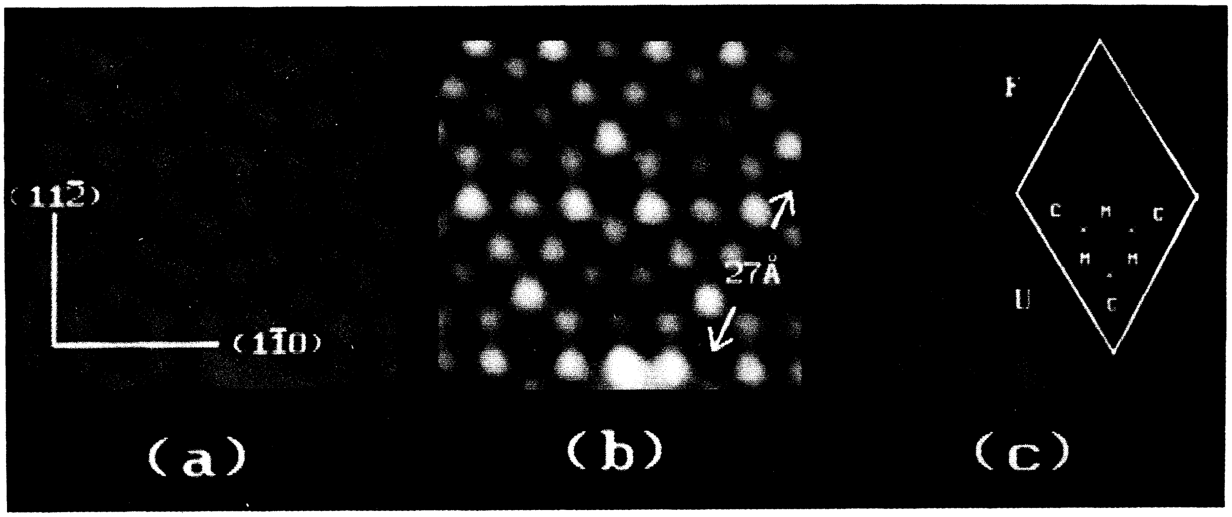

FIG. 2. Tunneling images of Si(111)-(7×7). (a) Unoccupied-state image (blue) taken at +1.0 V. (c) Occupied-state image (orange) taken at −1.0 V. (b) Superposition of the images shown in (a) and (c). The principal crystallographic directions are indicated, along with the image scale. *F* and *U* denote the faulted and unfaulted mesh halves, respectively. *C*, *M*, and *X* denote the positions of corner adatom, middle adatom, and rest-atom dangling bonds, respectively. The color saturation is keyed on height, with a range of 1.0 Å in (a) and 1.2 Å in (c). The demanded tunneling current was 1 nA for both images.

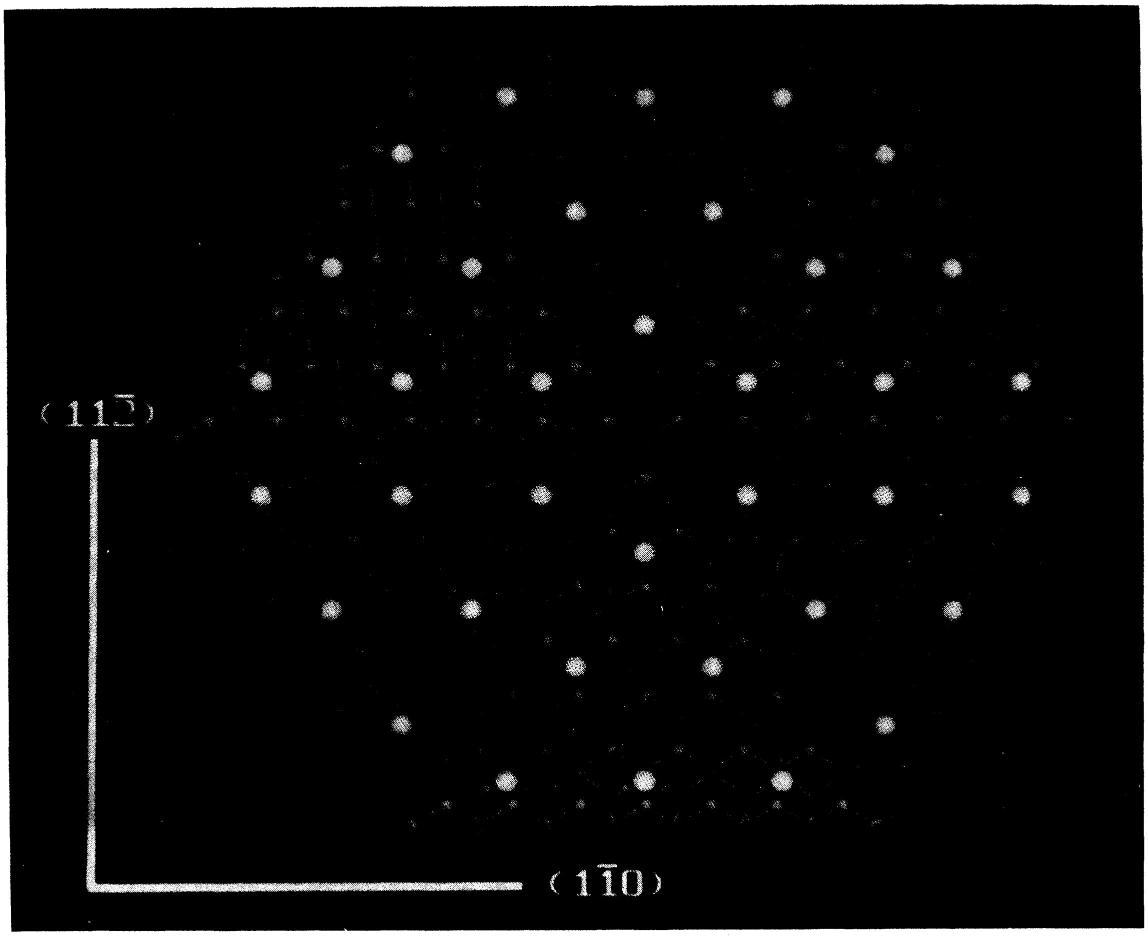

FIG. 3. Model of the dimer-adatom-stacking fault Si(111)-(7×7) surface. The colors for the rest atoms and substrate atoms for the faulted and unfaulted mesh halves are keyed to agree with the tunneling images in Fig. 2. Adatoms are in white, rest-atom dangling bonds in red, unfaulted backbond atoms in blue, faulted backbond atoms in orange, and dimerized domain wall atoms in magenta.

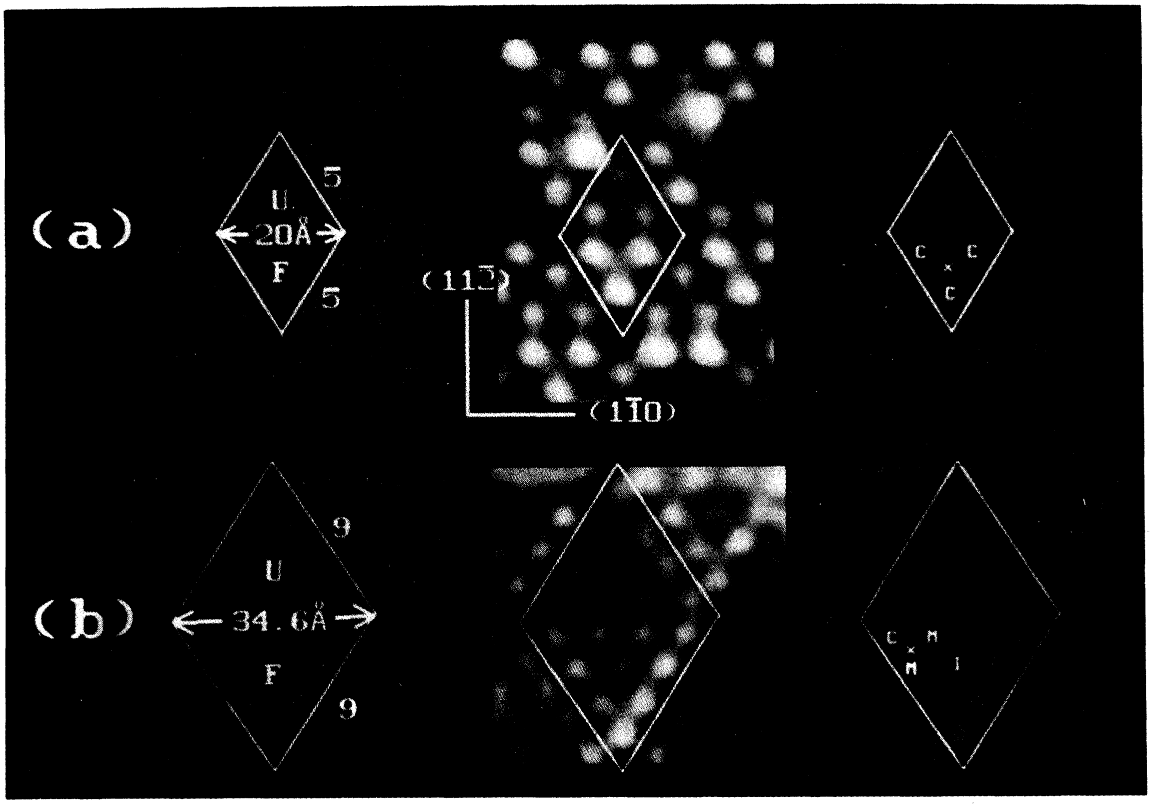

FIG. 4. Dual-polarity tunneling images for (a) Si(111)-(5×5) and (b) Si(111)-(9×9). The blue pictures represent unoccupied-state images while the orange images represent occupied-state images, with their superposition in the center as in Fig. 2. A unit mesh is outlined for the 5×5 and 9×9 with the principal crystallographic directions indicated. The *F* and *U* denote the faulted and unfaulted halves of the unit mesh. In the occupied-state (orange) images, the *C*, *M*, *I*, and *x* denote corner adatom, middle adatom, interior adatom, and rest-atom dangling bonds, respectively. The unoccupied-state image for the 5×5 was acquired at +1.5 V, the occupied-state image at −1.5 V. The 9×9 unoccupied-state image was acquired at +1.5 V and the occupied-state image at −1.7 V. All images were acquired at a demanded tunneling current of 1 nA. The color saturation is keyed on apparent height, with a dynamic range of ∼1 Å.

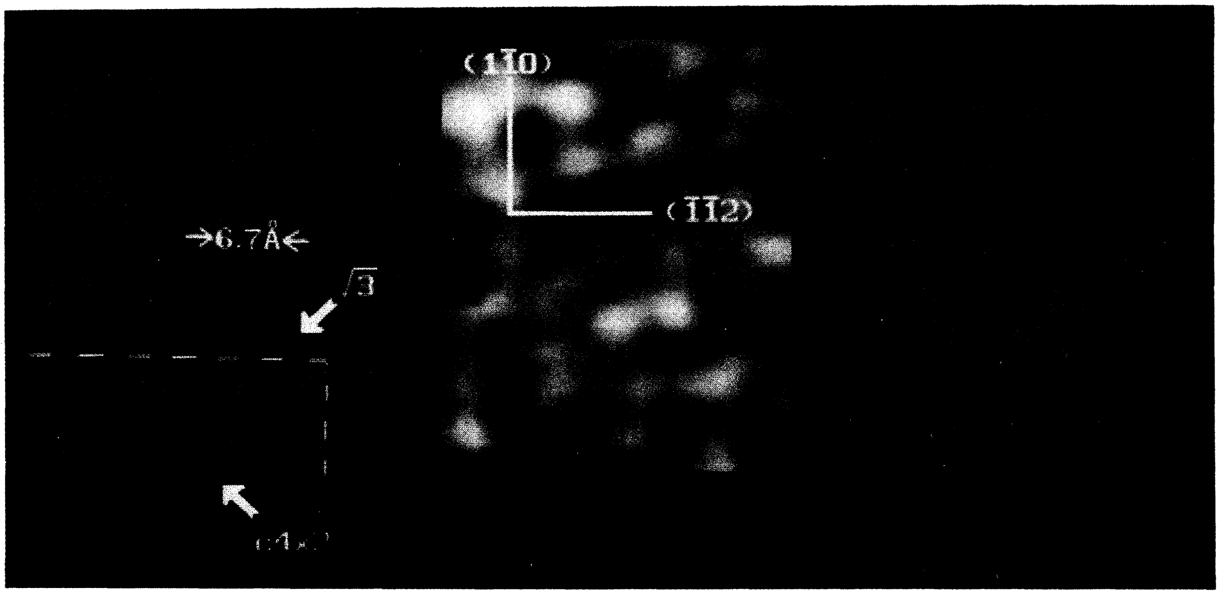

FIG. 5. Dual-polarity tunneling images for laser-stabilized Si(111). (a) Unoccupied-state image acquired at +1.0 V. (c) Occupied-state image acquired at −1.0 V bias. (b) Superposition of (a) and (c). The crystallographic directions and image scale are indicated. The arrow and dashed lines denote small regions of $c(4\times2)$ and $\sqrt{3}$ symmetry. The color saturation is keyed on height, with a range of 1.2 Å in (a) and 0.7 Å in (c). Both images were acquired at a tunneling current of 1 nA.

resolution images of the laser-stabilized Si(111) surface. The laser-stabilized Si(111) surface exhibits a 1×1 LEED pattern with a high background intensity. Detailed studies of this surface with LEED, photoemission, and infrared absorption spectroscopy failed to agree on the nature of the 1×1 LEED pattern with models ranging from the graphitelike 1×1 Si structure to a somewhat disordered 7×7 structure.[35] Initial work with the tunneling microscope revealed the nature of the surface: small regions of 2×2 and $c(4\times2)$ reconstructions, never more than a few unit meshes in size, distributed over the various twin configurations consistent with the threefold symmetry of the underlying lattice.[32] The small size of these structures prevented their identification by diffraction techniques, while the fact that structures with 2×2 and $c(4\times2)$ symmetry are incorporated into the 5×5, 7×7, and 9×9 unit meshes rendered the laser-stabilized and 7×7 surfaces nearly indistinguishable by photoemission or absorption spectroscopy. Further experimentation on this surface showed that a thermal anneal at 600 °C for a short period of time ($\sim$1 min) produces regions displaying the 5×5, 7×7, and 9×9 reconstructions interspersed with regions of 2×2 and $c(4\times2)$ symmetry. For this reason, it was concluded that the high-symmetry structures representing the laser-stabilized surface consisted of the adatoms of the Takayanagi-Tanishiro-Takahashi-Takahashi DAS model arranged on loosely packed T_4 sites, since the superposition of a 1×1 lattice on the tunneling images showed all the protrusions in the area to occupy the same category of site.

Figures 5(a)–5(c) show dual-polarity tunneling images obtained over the laser-stabilized Si(111) surface, with blue representing an image taken tunneling from the tip into empty sample states, while orange represents an image taken simultaneously tunneling from filled sample states to empty tip states. The arrows denote regions of local $c(4\times2)$ and $\sqrt{3}\times\sqrt{3}$ symmetry. In Fig. 5(b), we show the superposition of the filled- and empty-state images. Two features are immediately noticed: the filled-state image shows a relatively small amount of contrast ($\sim$0.4 Å) compared to the empty-state image, and the *positions of the protrusions do not superimpose,* in marked contrast to the tunneling images shown for the three DAS structures. It is interesting, at this point, to compare I-V characteristics of the tunnel junction for the Si(111)-(7×7) and the laser-stabilized Si(111)-(2×2) surface. These data, displayed as the ratio of the differential conductivity (dI/dV) divided by the total conductivity (I/V), are plotted in Fig. 6(a), along with similar data obtained on the Ge(111)-$c(2\times8)$ surface. This method of display has been demonstrated to give a qualitative representation of the surface density of states,[36] but suffers from the disadvantage of diverging at a band edge since the total conductivity can be quite small while the differential conductivity is large. Further, to lowest order, the quantity $(dI/dV)/(I/V)$ is proportional to $\rho/\int\rho$, where ρ is the local density of occupied or unoccupied states. Alternatively, the quantity $\log(dI/dV)$ can be plotted as in Fig. 6(b). This enables display of the junction characteristic to lower values of the bias voltage

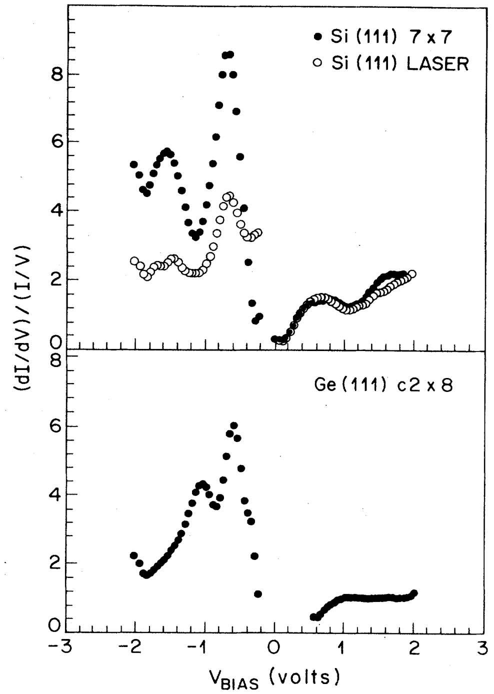

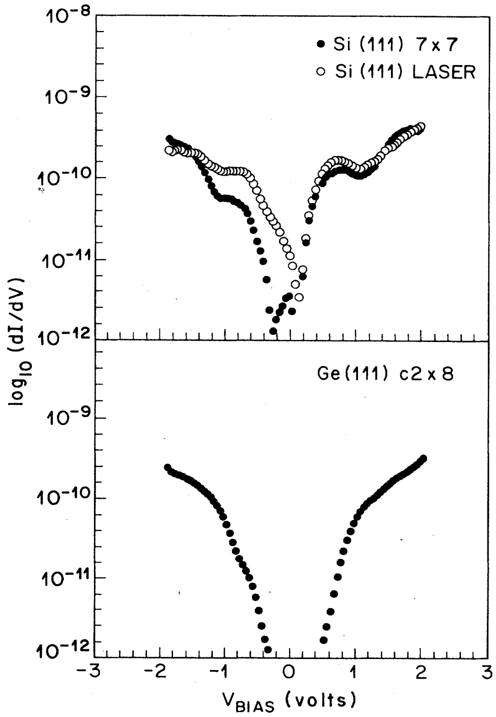

FIG. 6. (a) Differential over total conductivity for the tunnel junction I-V characteristics over Si(111)-(7×7), laser-stabilized Si(111), and Ge(111)-$c(2\times8)$. (b) $\log_{10}(dI/dV)$ for the same data sets as shown in (a).

V_b, giving a more accurate picture of any surface energy gap, while strong features (peaks) in $(dI/dV)/(I/V)$ now manifest themselves as shoulders. A more involved discussion of the correspondence of the features in tunnel junction I-V characteristics and the local density of states has been presented by Lang.[37] In both Figs. 6(a) and 6(b), positive values of the bias voltage correspond to tunneling from the tip into empty sample states while negative values correspond to tunneling from filled sample states into empty tip states. The similarity of the data for the two Si surfaces is striking and merits comment at this point, while the data for the Ge(111) surface will be discussed later. For unoccupied sample states, both the 7×7 and the disordered (2×2) Si(111) surfaces show a peak at $+0.4$ V identified from inverse photoemission[38] and earlier STM work[16] as a dangling-bond state. The unoccupied state at $\sim+1.5$ V is a feature related to the partial stacking fault on the 7×7, identified in early differential conductivity work performed with the STM on the 7×7 superstructure.[39] It is noted that this feature is nearly nonexistent for the laser-stabilized 2×2 surface. The occupied sample-state side of the normalized differential conductivity can be more difficult to interpret since features here may be convolved with empty tip states.[28,29] The features discussed here are generally present in I-V characteristics acquired with a relatively low contrast tip, and are strong enough to dominate tip states. The peak at -0.8 V for both the Si-(7×7) and -(2×2) data is tentatively identified as a dangling-bond state, the S_2 state seen in detailed photoemission studies of the 7×7.[33] The feature at -1.5 to -1.6 V, in similar fashion, corresponds to the photoemission S_3 state. The S_1 state, lying at ~0.2 V, is not unambiguously seen in either Si(111) data set, but the logarithmic display of the differential conductivity in Fig. 6(b) shows no clear energy gap down to 10^{-12} A/V, indicating filled states just below E_F may be present. The detection of state density near E_F is difficult to determine unambiguously with the STM since the tunnel current I vanishes as V_b approaches zero. We see that the overall features are similar, indicating that the 2×2 geometry present on both the Si(111) laser-stabilized and the 7×7 structures dominates the measured electronic structure. This is in good agreement with UPS studies[40,41] that show the two surfaces to be electronically similar.

Since the junction I-V characteristics for the Si(111)-(7×7) and the disordered 2×2 structures are very similar, it is natural to extend the calculations and arguments of Northrup to the high-symmetry 2×2 and $c(4\times2)$ structures on the laser-stabilized surface. For the 2×2 unit mesh, described as adatoms loosely populating a 1×1 substrate, there are two dangling bonds: one rest atom and one adatom. This yields a completely filled rest-atom band and an empty adatom band. Similarly, for the $c(4\times2)$, we have four dangling bonds distributed over two rest atoms and two adatoms, again resulting in a filled rest-atom band and an empty adatom band. From this argument, the dual-polarity tunneling images of the laser-stabilized Si(111) surface should fail to show superimposed protrusions if the surface structure is described by adatoms on T_4 sites arrayed on 2×2 boundaries on a 1×1 substrate. This is clearly consistent with the tunneling images in Fig. 5. Further, on the partially reannealed surface, the presence of surface reconstructions incorporating the DAS geometry is immediately discernible in an examination of superimposed dual-polarity tunneling images. This effect is illustrated in Figs. 7(a) and 7(b), showing regions of the laser-stabilized Si(111) surface that have local symmetries of 5×5 and 7×7 DAS intermixed with adjacent regions of 2×2 and $c(4\times2)$ symmetry. In these images, superposition of protrusions is clearly seen when the DAS geometry is taken up, with no superposition detected in the 2×2 and $c(4\times2)$ regions. This set of tunneling images clearly illustrates the STM's sensitivity to changes in electronic structure on the scale of a few tens of atoms.

Having demonstrated the detailed dependence of the contrast in the tunneling image, especially when tunneling from filled sample states just below E_F into empty tip states, to the symmetry displayed by the protrusions on the (111) silicon surfaces, we are now ready to consider our images of the Ge(111) surface. The tunneling image shown in Fig. 1 acquired tunneling into empty sample states clearly displays local symmetry consistent with that shown in analogous images acquired on laser-stabilized Si(111), but with a somewhat longer range in the ordering. Figure 8(a) shows a dual-polarity tunneling image of Ge(111)-$c(2\times8)$ surface, while Fig. 8(b) shows a similar, higher sampling density image of a mixed 2×2 and $c(4\times2)$ region. It is immediately seen that we have a complete separation of the empty-state (blue) and filled-state (orange) images, precisely as shown for the laser-stabilized Si(111) surface in the regions of reconstructed 2×2 and $c(4\times2)$ structures. Further examination of the images in Fig. 8 shows the presence of protrusions in the occupied-state images (orange) in between the protrusions in the unoccupied-state images (blue) in the regions of $c(4\times2)$ symmetry, in direct contrast to the superposition seen in the seemingly $c(4\times2)$ dimer domain boundaries in the DAS structures. Moreover, the orientation of the substrate, determined by Laue x-ray measurements, shows the relative positions of protrusions in both the empty- and filled-state images to be consistent with adatoms occupying T_4 sites on a 1×1 substrate. In this configuration the adatoms are associated with the unoccupied dangling-bond states while the occupied dangling-bond state is associated with the rest atoms. This is illustrated in Fig. 9 where ball-and-stick models for the Ge(111) $c(2\times8)$ surface are shown at the same orientation for (a) T_4 site adatoms on a 1×1 substrate, and (b) the Takayanagi-Tanishiro dimer-chain model for the $c(2\times8)$ reconstruction.[42] Here, adatoms are shown in blue and rest-atom dangling bonds are displayed in red, to be consistent with the data in Fig. 8.

DISCUSSION

Ge(111) surface reconstruction

The principal discrepancy between the dimer-chain (DC) model for the $c(2\times8)$ structure and the tunneling images shown in Fig. 8 is that it fails to account for the

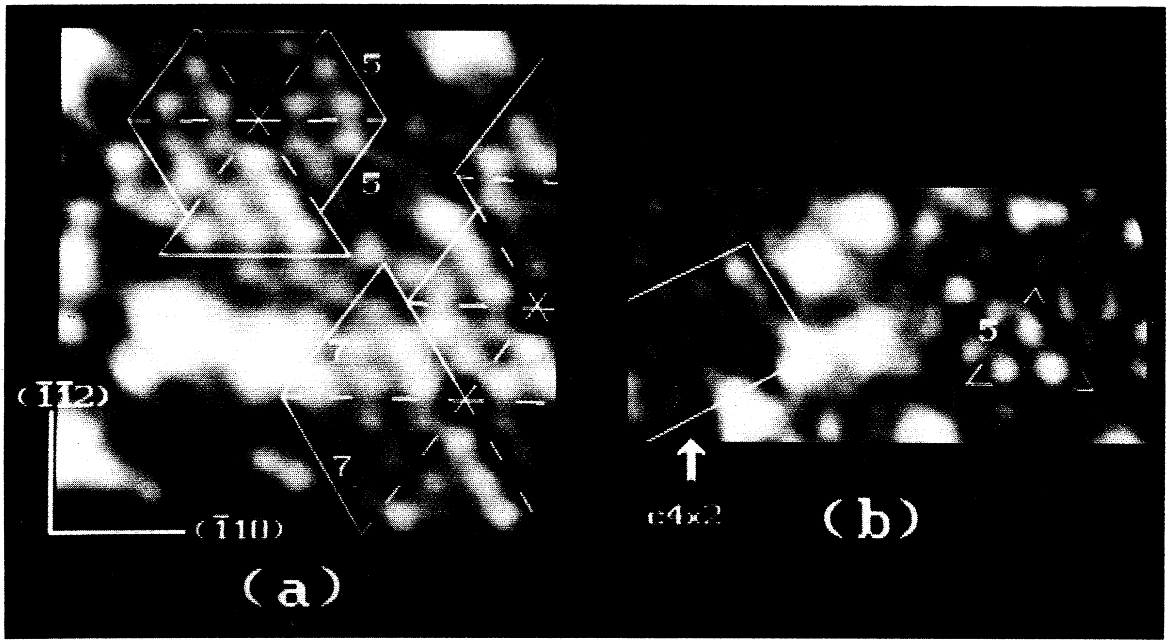

FIG. 7. Superimposed dual-polarity tunneling images for laser-stabilized and partially reannealed Si(111). Blue represents the unoccupied-state image, orange represents the filled-state image, while white indicates both. The solid and dashed lines in (a) denote regions of 5×5 and 7×7 symmetry reconstructed in the DAS fashion. The solid lines in (b) enclose a region of $c(4\times2)$ symmetry while the dashed lines denote a DAS 5×5 mesh. The principal crystallographic directions are indicated. These images were acquired at 1.5 V bias and 1.0 nA tunneling current in both polarities.

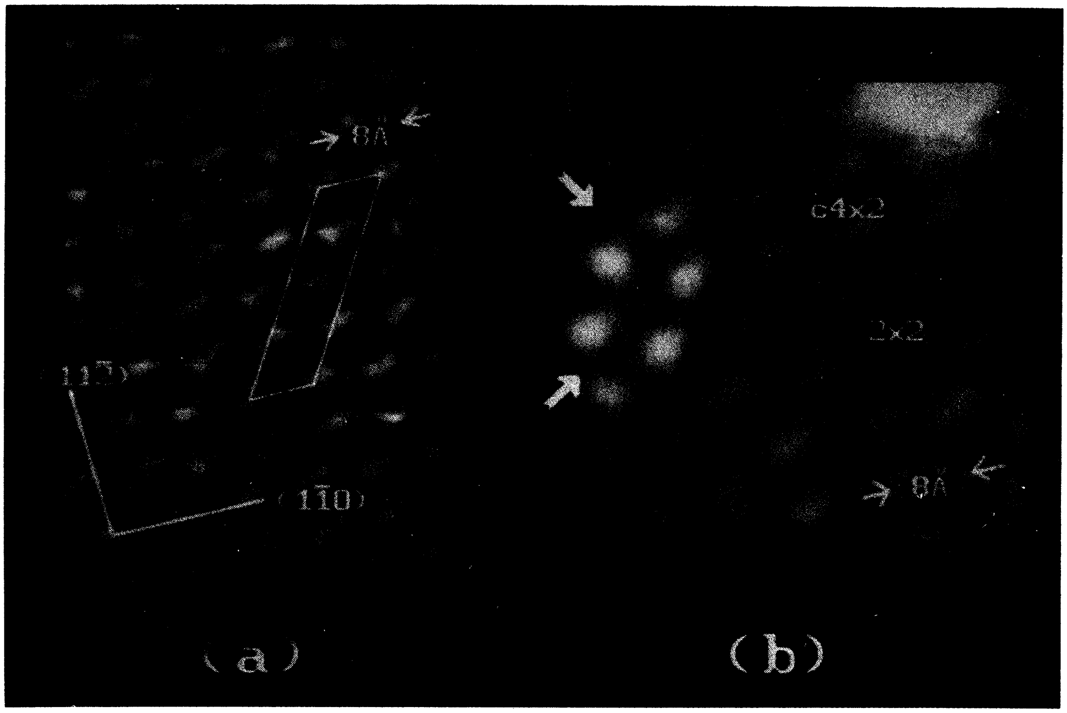

FIG. 8. Superimposed dual-polarity tunneling images for (a) the Ge(111)-$c(2\times8)$ surface, and (b) 2×2, $c(4\times2)$, and $\sqrt{3}\times\sqrt{3}$ domains. Blue represents the unoccupied-state image, orange the occupied-state image, and white both. The principal crystallographic directions are indicated. The solid lines enclose a $c(2\times8)$ unit mesh in (a). The arrows denote a local region of $\sqrt{3}$ symmetry in (b) large enough to show unoccupied-occupied state superposition. Local regions of 2×2 and $c(4\times2)$ symmetry are indicated. The unoccupied-state image was acquired at +2.0 V and the occupied-state image at −2.0 V 1.0 nA demanded tunneling current. The color saturation is keyed on height, with a range of 0.8 Å for the unoccupied-state image and a range of 0.5 Å for the occupied-state image.

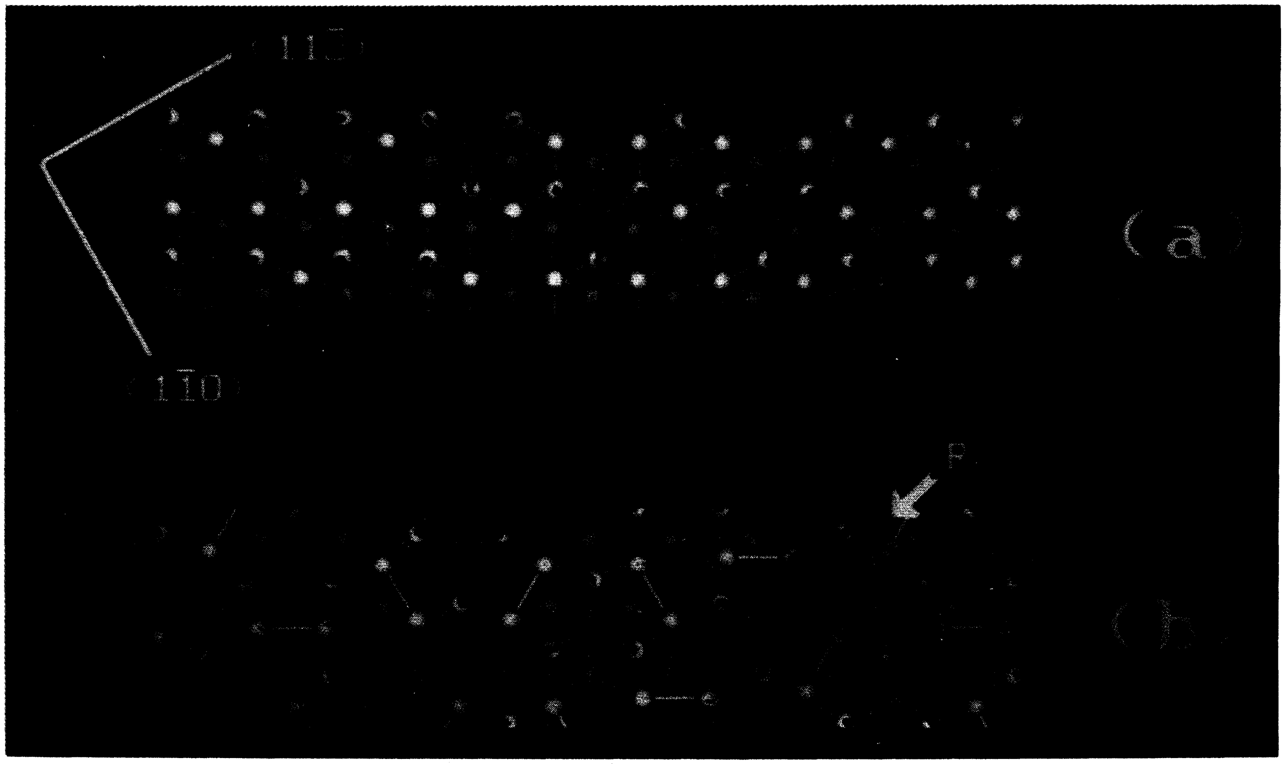

FIG. 9. Ball-and-stick models for the Ge(111)-$c(2\times8)$ surface. (a) Simple adatom phase. (b) Takayanagi dimer-chain adatom phase. Blue denotes adatom and orange denotes rest-atom dangling bonds. The heavy black lines and the R in (b) denote an eight-member ring similar to those in the dimer walls in the DAS reconstructions.

spatial shift between the empty- and filled-state images. Since the DC model essentially consists of alternating strips of faulted and unfaulted substrates which are more narrow than two lattice spacings when the transition dimer regions are included, there are no rest-atom dangling bonds on the substrate (all substrate Ge atoms are either dimerized or bonded to an adatom). In this geometry, the only dangling bonds are on the adatoms, implying a half-filled dangling-bond band. As in the DAS structures, superposition between the empty- and filled-state tunneling images would then be expected, but is not observed. Further, a partially filled dangling-bond surface band is in contradiction to photoemission measurements for this surface[4,9–12] which show it to be semiconducting. In contrast, a simple model of adatoms on T_4 sites loosely arranged in 2×2 and $c(4\times2)$ configurations is entirely consistent with the tunneling images and photoemission experiments. In fact, this local 2×2 geometry is also realized by the interior (I) adatoms in the 9×9 cell. This adatom is surrounded by three rest atoms and essentially vanishes in the filled-state image [Fig. 4(b)], just as the adatoms on Ge(111)-(2×8). Also consistent with this model is the small region of $\sqrt{3}\times\sqrt{3}$ symmetry indicated by arrows in Fig. 8(b). This region images with superimposed filled and empty states on the adatom positions, which is exactly as expected for a purely $\sqrt{3}\times\sqrt{3}$ arrangement of adatoms on a 1×1 substrate. The existence of disordered step risers also supports a simple adatom picture. Referring to Fig. 1, which shows an empty-state tunneling image of Ge(111)-$c(2\times8)$, we note that the two double-layer steps are neither reconstructed as previously reported for Si(111)-(7×7) (Ref. 15) and -(2×1) (Ref. 30) steps, nor do they lie on principal crystallographic directions. Rather, the Ge(111) surface incorporates the subelements of the $c(2\times8)$, 2×2, and $c(4\times2)$ surfaces, as needed at the step riser as does the laser-stabilized Si(111) surface.[32] This example of step structure, consistent with a simple 1×1 substrate, is more difficult to reconcile with any surface configuration involving considerable substrate reconstruction. The absence of long-range order on the Ge(111)-$c(2\times8)$ surface, in contrast to the Si(111)-(7×7) surface, indicates there are only small energy differences between the various configurations seen in the tunneling images, while the failure to reconstruct atomic steps, resulting in large numbers of dangling bonds, may account for some of the greater reactivity of the equilibrium Ge(111) surface. Additional evidence against the DC model comes from recent calculations where both tight-binding energy minimization[43] and a new dimer-wall-formation energy-minimization model proposed by Vanderbilt[44] indicate that the DC model for the $c(2\times8)$ has far too high a formation energy. Vanderbilt further argues that since a dense pattern of parallel rows of dimer walls is topologically impossible, the zigzag arrangement of dimers in the DC model is demanded, generating double the number of dimers per unit length and resulting in too high a strain energy. This is a direct result of the fact that the underlying lattice is threefold symmetric, not sixfold symmetric.

The only evidence against a simple adatom phase consists of Rutherford backscattering (RBS) experiments performed on Ge(111)-$c(2\times8)$ surfaces.[45] The RBS measurements registered large blocking peaks at off-normal incidence which have been interpreted as arising from the presence of at least a partial stacking fault as in the case of Si(111)-(7×7). However, this analysis was based on the assumption of adatoms occupying H_3 (open) sites, not T_4 (closed) sites, and does not include scattering power arising from such factors as mixed surface phases, defects, and steps. Impact collision ion scattering spectra of the Ge(111)-$c(2\times8)$ surface are significantly different from similar spectra on the Si(111)-(7×7) surface and do not show strong surface focusing peaks.[46] Further, the presence of a stacking fault over the entire Ge(111) surface is inconsistent with the presence of *single* double-layer steps, since an energy cost would have to be paid for the destruction of the fault at the lower edge of each step riser. We note that the equilbrium 7×7 surface, prepared by annealing at temperatures of over 900 °C, tends to display multiple double-layer steps consisting of six to ten double layers with small terraces of 10–15 Å width between step risers, while we have only detected single double-layer steps on similar Ge(111)-$c(2\times8)$ and laser-stabilized Si(111) surfaces. These small terraces on the equilibrium Si(111) surface are narrow enough for the DAS reconstruction to be discarded in favor of a simple adatom phase similar to Ge(111), while the destruction energy for the partial stacking fault at the 7×7 surface has to be paid only once for the step array. Further, comparison of the I-V characteristics shown in Fig. 6 for the three $\langle 111 \rangle$ surfaces shows that the prominent unoccupied state at +1.5 V associated with the stacking fault in the Si(111)-(7×7) surface is absent in the I-V data for the laser-stabilized Si(111) and the Ge(111)-$c(2\times8)$ surfaces. Finally, we note that in images of the laser-stabilized and partially reannealed Si(111) surface, DAS and non-DAS structures exist simultaneously and contiguously. Extension of a 1×1 lattice over the images shows all adatoms occupy the same category of site, T_4. For these reasons, we cannot support a model consisting of H_3 adatoms on a 1×1 faulted substrate.

Geometric contribution to contrast

Up to this point we have only considered electronic contributions to the contrast in the tunneling images. An additional source of contrast could arise from the geometric height of the various atomic features upon which the empty and filled states are localized. When first analyzing the data, we thought that this effect might be contributing to the tunneling images of the laser-stabilized Si(111) and the Ge(111)-$c(2\times8)$ surfaces. For these surfaces we find that the contrast in the images derived from unoccupied states (0.6 Å on average) is similar to that measured in unoccupied-state images for Si(111)-(7×7) (0.5–1.0 Å), while the contrast in the analogous filled-state images is typically much less (0.25 Å on average). We point out that measured values for the contrast at a given bias condition for these semiconductors can vary by a factor of 2, depending on the tunneling tip. The values reported here are representative of many images acquired on these surfaces. However, the following exercise demonstrates that any contrast on *periodic* and atomically flat semiconductor surfaces that is greater than a few 0.01 Å must be due to electronic contributions and not to the physical height of the surface atoms. This, of course, does not apply at step edges or at many-atom-high protrusions.

For a simple 2×2 adatom configuration on a 1×1 substrate, the unoccupied dangling-bond states are localized on the geometrically higher adatoms, while the filled dangling-bond states are associated with the rest atoms in between. If we assume that the density of states for the unoccupied and occupied dangling-bond bands are similar, the difference in corrugation would be due to the effective height of the adatoms *at the position of the tip*, which is approximately 8–10 Å above the surface at a tunneling impedance of 1 GΩ. In this approximation, the effective height of the adatoms is roughly half of the difference in corrugation amplitude, as the local surface curvature increases the corrugation for states associated with adatoms, while decreasing the corrugation for states located at the rest-atom positions between the adatoms. This gives a value of ~0.2 Å for the geometric contribution to the adatom corrugation at the height of the tunneling tip. For comparison, early STM work on Au(110) reported a corrugation amplitude of 0.45 Å for the 2×1 missing-row structure[47] which possesses a comparable lateral distance scale of 8 Å. The results of that work were well explained by the theory of Tersoff and Hamann, who derived an effective tip radius of 9 Å with a gap of 6 Å at a tunneling impedance of 10 MΩ.[21] While that treatment is not strictly applicable in the present case (since the bias voltage V_b is not much less than the work function ϕ), it is nonetheless instructive to attempt to explain the excess contrast of 0.2 Å as a geometric feature. Tersoff and Hamann demonstrated that the measured corrugation for periodic structures decreases approximately exponentially with vacuum gap. Since the vacuum gap is ~2 Å greater for the bias conditions in this work, we calculate a geometric corrugation of 0.01–0.02 Å for the 2×2 adatom geometry, an order of magnitude lower than the residual 0.2 Å in this rough analysis. Therefore, our assumption that the densities of state are similar for the unoccupied and occupied dangling-bond bands cannot be valid, i.e., even the residual 0.2 Å is related to differences in state density and/or electronic structure. We conclude that the measured corrugations in tunneling images of periodic semiconductors is derived almost entirely from electronic state density, rendering tunneling image simulation by atomic charge superposition[24] unphysical for semiconductors.

Surface-electronic characteristics

The I-V characteristics displayed in Figs. 6(a) and 6(b) for the Si(111)-(7×7), the disordered Si(111)-(2×2), and the Ge(111)-$c(2\times8)$ surface phases are generally similar, but have detailed differences relating to their respective subsurface structure. In contrast to the laser-stabilized Si(111) characteristic, which in peak positions is quite similar to the 7×7 characteristic, the Ge(111)-$c(2\times8)$ surface shows a single unoccupied state at $+0.6$ V, similar to the peaks at $+0.4$ V on the two Si(111) surfaces, which we attribute to an adatom dangling-bond band. A feature at -0.7 V and another at -1.2 V are seen, close to the prominent surface bands at -0.85 and -1.4 V that have been reported in several UPS studies.[4,9–12] Following the labeling for the qualitatively similar Si(111) features, these are attributed to rest-atom dangling bonds and adatom backbonds, respectively, keeping in mind the previous caveat concerning occupied sample states' I-V characteristics. No evidence was detected for features near E_F as shown in Fig. 6(b), indicating the surface is semiconducting. Indeed, the plot of $\log_{10}(dI/dV)$ presented in Fig. 6(b) for the Ge(111)-$c(2\times8)$ surface shows a clear energy gap. In the simple adatom phase model, there exist three distinct environments for adatoms and rest-atom dangling bonds: purely 2×2 domains, purely $c(4\times2)$ domains, and $c(2\times8)$ domains where both rest atoms and adatoms are always bounding both 2×2 and $c(4\times2)$ domains (mixed symmetry). This may be responsible for the "triplet" feature reported at certain takeoff angles in ARUPS experiments by Yokotsuka *et al.*[4]

We note in passing that in studies on laser-stabilized Si(111) surfaces we have seen a number of small areas of $\sqrt{3}\times\sqrt{3}$ symmetry which are imaged in the same manner as that displayed in the tunneling image in Fig.

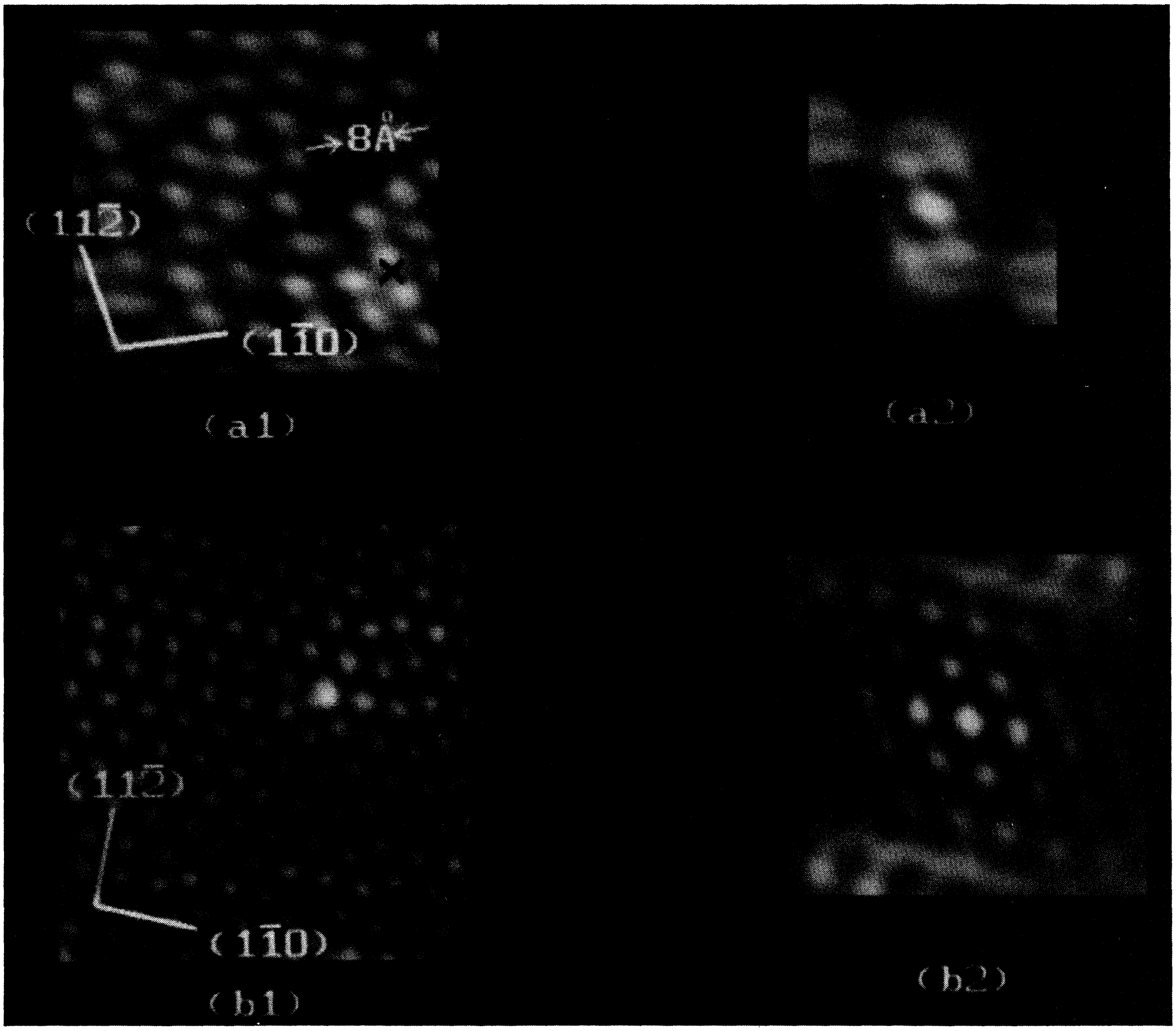

FIG. 10. Tunneling images and their autocorrelations for laser-stabilized Si(111) [(a1) and (a2)], and Ge(111) [(b1) and (b2)]. The crystallographic directions are indicated along with the scale for both images. The X denotes a large region of $\sqrt{3}$ symmetry.

8(b). These small regions of $\sqrt{3}\times\sqrt{3}$ symmetry may be responsible for the small contributions to the tunneling current seen in the I-V data set in Fig. 6 for the laser-stabilized Si(111) surface, which has been integrated over a number of regions. We note that this is in contrast to reported UPS studies of the laser-stabilized Si(111)-(1×1) and Si(111)-(1×1)H surfaces,[40,41] where no state close to E_F was detected on the laser-stabilized surface, while the S_2 and S_3 surface states of the Si(111)-(7×7) surface were seen. The UPS results are consistent with a disordered 2×2 adatom array with no significant regions of $\sqrt{3}\times\sqrt{3}$ symmetry. Close examination of the I-V data in Fig. 6 for the laser-stabilized Si(111) surface shows no clearly discernible feature in close proximity to E_F as has been reported in several STM studies on Si(111)-(7×7), and in fact can be seen to some extent in the Si(111)-(7×7) I-V data shown in Fig. 6. The relative amount of order on laser-stabilized Si(111) and equilibrium Ge(111) surfaces is illustrated in Fig. 10. Figures 10(a1) and 10(a2) show a typical 70 Å region of the laser-stabilized Si(111) surface and its autocorrelation, respectively. The autocorrelation shows there to be some ordering, indicated by a bright ring surrounding the central maxima. Upon closer examination, this ring is found to have some intensity located at a $\sqrt{3}\times\sqrt{3}$ spacing along $[11\bar{2}]$ from the central maxima, indicating a small amount of nearest-neighbor adatom spacing at this distance. Additional maxima are located at two lattice spacings along the $[1\bar{1}0]$ directions denoting ordering of 2×2 symmetry. Inspection of the tunneling image in Fig. 10(a1) shows significant groupings of $\sqrt{3}\times\sqrt{3}$ symmetry, with a small contiguous region indicated at ×. In contrast, in Fig. 10(b1) we show a typical Ge(111) surface, with the corresponding autocorrelation in Fig. 10(b2). Here, it is obvious that the principal ordering is along $\langle 110\rangle$ directions with a spacing of two lattice vectors. Indeed, it can be seen that good order is maintained out to approximately the fourth-nearest-neighbor distance. It is clear from the autocorrelations in Fig. 10 that the laser-stabilized Si(111) surface is more disordered than a typical Ge(111) surface. We have never seen a complete sixfold ring of $\sqrt{3}\times\sqrt{3}$ symmetry, indicating that the lattice strain is too great to support such a structure with Si and Ge adatoms, in contrast to the $\sqrt{3}\times\sqrt{3}$ symmetry displayed by numerous metal overlayers. It is possible that the alternation of 2×2 and $c(4\times2)$ strips in the $c(2\times8)$ structure is the result of a strain-relieving mechanism in the adatom-substrate atom bonds, perhaps related to that proposed by McRae for Si(111)-(7×7).[48]

CONCLUSION

In summary, we have examined in detail the closely related surface reconstructions of Si(111)-(5×5), -(7×7), -(9×9), laser-stabilized disordered Si(111)-(2×2), and Ge(111)-$c(2\times8)$. We find the tunneling images for the 5×5, 7×7, and 9×9 structures to be well described by the Takayanagi-Tanishiro-Takahashi-Takahashi DAS model, while the laser-stabilized Si(111) and the Ge(111)-$c(2\times8)$ surfaces are consistent with adatoms occupying T_4 sites in a loosely packed 2×2 array on a 1×1 substrate. The 5×5 structure is shown to be nearly "pure" DAS-like with one species of adatom, while the 9×9 structure has three adatom species and exhibits some of the characteristics of the laser-stabilized Si(111) and the Ge(111)-$c(2\times8)$ surfaces. We have found no evidence supporting the presence of a full or partial stacking fault on the Ge(111) equilibrium surface. A comparison of the filled- and empty-state tunneling images and junction I-V characteristics with recent pseudopotential calculations by Northrup gives good agreement, with the images interpreted essentially as the spatial position of filled and empty surface dangling bonds. Finally, we find that the apparent heights of the adatoms in the tunneling images of these adatom reconstructions are derived almost entirely from the electronic as opposed to the geometric structure of the surface.

ACKNOWLEDGMENTS

In the course of preparation of this work we would like to acknowledge fruitful discussions with D. R. Hamann, J. E. Rowe, Y. J. Chabal, J. R. Patel, M. S. Hybertsen, and Y. Kuk of AT&T Bell Laboratories and J. A. Golovchenko of Harvard University.

---

*Present address: University of Wisconsin–Madison, Madison, WI 53706.

[1] K. Takayanagi, Y. Tanishiro, M. Takahashi, and S. Takahashi, J. Vac. Sci. Technol. A **3**, 1502 (1985).

[2] H. J. Gossman, J. C. Bean, L. C. Feldman, and W. M. Gibson, Surf. Sci. **138**, L175 (1984); E. G. McRae, H. J. Gossman, and L. C. Feldman, *ibid.* **146**, L540 (1984).

[3] R. S. Becker, J. A. Golovchenko, and B. S. Swartzentruber, Phys. Rev. B **32**, 8455 (1985).

[4] T. Yokotsuka, S. Kono, S. Suzuki, and T. Sagawa, J. Phys. Soc. Jpn. **53**, 696 (1984).

[5] S. B. DiCenzo, P. A. Bennet, D. Tribula, P. Thiry, G. K. Wertheim, and J. E. Rowe, Phys. Rev. B **31**, 2330 (1985).

[6] R. S. Becker, B. S. Swartzentruber, and J. S. Vickers, J. Vac. Sci. Technol. A **6**, 472 (1988).

[7] P. W. Palmberg and W. T. Peria, Surf. Sci. **6**, 57 (1967).

[8] D. J. Chadi and C. Chiang, Phys. Rev. B **23**, 1843 (1981); W. S. Yang and F. Jona, *ibid.* **29**, 899 (1984); R. J. Phaneuf and M. B. Webb, Surf. Sci. **164**, 167 (1985).

[9] R. D. Bringans and H. Hochst, Phys. Rev. B **25**, 1081 (1982).

[10] J. M. Nicholls, G. V. Hansson, and R. I. G. Uhrberg, Phys. Rev. B **33**, 5555 (1986).

[11] R. D. Bringans, R. I. G. Uhrberg, and R. Z. Bachrach, Phys. Rev. B **34**, 2373 (1986).

[12] J. Aarts, A. J. Hoeven, and P. K. Larsen, Phys. Rev. B **37**, 8190 (1988).

[13] R. S. Becker, J. A. Golovchenko, and B. S. Swartzentruber, Phys. Rev. Lett. **54**, 2678 (1985).

[14] G. Binnig, H. Rohrer, Ch. Gerber, and E. Weibel, Phys. Rev. Lett. **50**, 120 (1983).

[15] R. S. Becker, J. A. Golovchenko, E. G. McRae, and B. S. Swartzentruber, Phys. Rev. Lett. **55**, 2028 (1985).

[16] R. J. Hamers, R. M. Tromp, and J. E. Demuth, Phys. Rev. Lett. **56**, 1972 (1986).

[17] Th. Berghaus, A. Brodde, H. Neddermeyer, and St. Tosch, J. Vac. Sci. Technol. A (to be published); Surf. Sci. **193**, 235 (1988).

[18] In operation, the scanning head of this STM is similar to that described in K. Besocke, Surf. Sci. **181**, 145 (1987).

[19] A. Ishizaka, N. Nakagawa, and Y. Shiraki, in *Proceedings of the Second International Symposium on Molecular Beam Epitaxy and Related Clean Surface Techniques* (Japan Society of Applied Physics, Tokyo, 1982), p. 183.

[20] Surface-cleaning and -annealing recipes that result in Si(111) reconstructing in a 5×5 as opposed to 7×7 manner have been reported in early investigations with LEED on these surfaces. See, for example, J. J. Lander, G. W. Gobeli, and J. Morrison, J. Appl. Phys. **34**, 2298 (1963).

[21] J. Tersoff and D. R. Hamann, Phys. Rev. Lett. **50**, 1998 (1983).

[22] Y. Kuk and P. J. Silverman, J. Vac. Sci. Technol. A (to be published).

[23] R. J. Hamers, R. M. Tromp, and J. E. Demuth, Surf. Sci. **181**, 346 (1987).

[24] R. M. Tromp, R. J. Hamers, and J. E. Demuth, Phys. Rev. B **34**, 1388 (1986).

[25] J. A. Stroscio, R. M. Feenstra, and A. P. Fein, J. Vac. Sci. Technol. A **5**, 838 (1987).

[26] J. A. Stroscio, R. M. Feenstra, and A. P. Fein, Phys. Rev. Lett. **57**, 2579 (1986).

[27] R. M. Feenstra, J. A. Stroscio, J. Tersoff, and A. P. Fein, Phys. Rev. Lett. **58**, 1192 (1987).

[28] J. A. Kubby, J. E. Griffith, R. S. Becker, and J. S. Vickers, Phys. Rev. B **36**, 6079 (1987).

[29] R. S. Becker, T. Klitsner, and J. S. Vickers, Phys. Rev. B **38**, 3537 (1988).

[30] R. M. Feenstra and J. A. Stroscio, Phys. Rev. Lett. **59**, 2173 (1987).

[31] P. E. Wierenga, J. A. Kubby, and J. E. Griffith, Phys. Rev. Lett. **59**, 2169 (1987).

[32] This effect in the unoccupied state tunneling images of Si(111) 9×9 was noted earlier and attributed to electronic-structure differences between the interior adatom and the other adatoms. R. S. Becker, J. A. Golovchenko, G. S. Higashi, and B. S. Swartzentruber, Phys. Rev. Lett. **57**, 1020 (1986).

[33] P. Mårtensson, A. Cricenti, L. S. O. Johansson, and G. V. Hansson, Phys. Rev. B **34**, 3015 (1986); P. Mårtensson, W.-X. Ni, G. V. Hansson, J. M. Nicholls, and B. Reihl, *ibid.* **36**, 5974 (1987).

[34] J. E. Northrup, Phys. Rev. Lett. **57**, 154 (1986).

[35] There is an extensive body of literature on the details of the laser-annealed Si(111) surface. See, for example, R. M. Tromp, E. J. van Loenen, M. Iwami, and F. Saris, Solid State Commun. **44**, 971 (1980); D. M. Zehner, J. R. Noonan, H. L. Davis, and C. W. White, J. Vac. Sci. Technol. **18**, 852 (1981); F. Jona, P. M. Marcus, H. L. Davis, and J. R. Noonan, Phys. Rev. B **33**, 4005 (1986); Y. J. Chabal, G. S. Higashi, and S. B. Christman, *ibid.* **28**, 4472 (1983); W. S. Yang and F. Jona, *ibid.* **28**, 1178 (1983).

[36] J. A. Stroscio, R. M. Feenstra, and A. P. Fein, Phys. Rev. Lett. **57**, 2579 (1986).

[37] N. D. Lang, Phys. Rev. B **34**, 5947 (1986).

[38] J. M. Nicholls and B. Reihl, Phys. Rev. B **36**, 8071 (1987).

[39] R. S. Becker, J. A. Golovchenko, D. R. Hamann, and B. S. Swartzentruber, Phys. Rev. Lett. **55**, 2032 (1985).

[40] D. M. Zehner, C. W. White, P. Heimann, B. Reihl, F. J. Himpsel, and D. E. Eastman, Phys. Rev. B **24**, 4875 (1981).

[41] Y. J. Chabal, J. E. Rowe, and D. A. Zwemer, Phys. Rev. Lett. **46**, 600 (1981).

[42] K. Takayanagi and Y. Tanishiro, Phys. Rev. B **34**, 1034 (1986).

[43] G.-X. Qian and D. J. Chadi, Phys. Rev. B **35**, 1288 (1987).

[44] D. Vanderbilt, Phys. Rev. B **36**, 6209 (1987).

[45] R. J. Culbertson, Y. Kuk, and L. C. Feldman, Surf. Sci. **167**, 127 (1986).

[46] K. Sato, Surf. Sci. **158**, 644 (1985).

[47] G. Binnig, H. Rohrer, Ch. Gerber, and E. Weibel, Surf. Sci. **131**, L379 (1983).

[48] E. G. McRae, Phys. Rev. B **28**, 2305 (1983); Surf. Sci. **147**, 663 (1984).

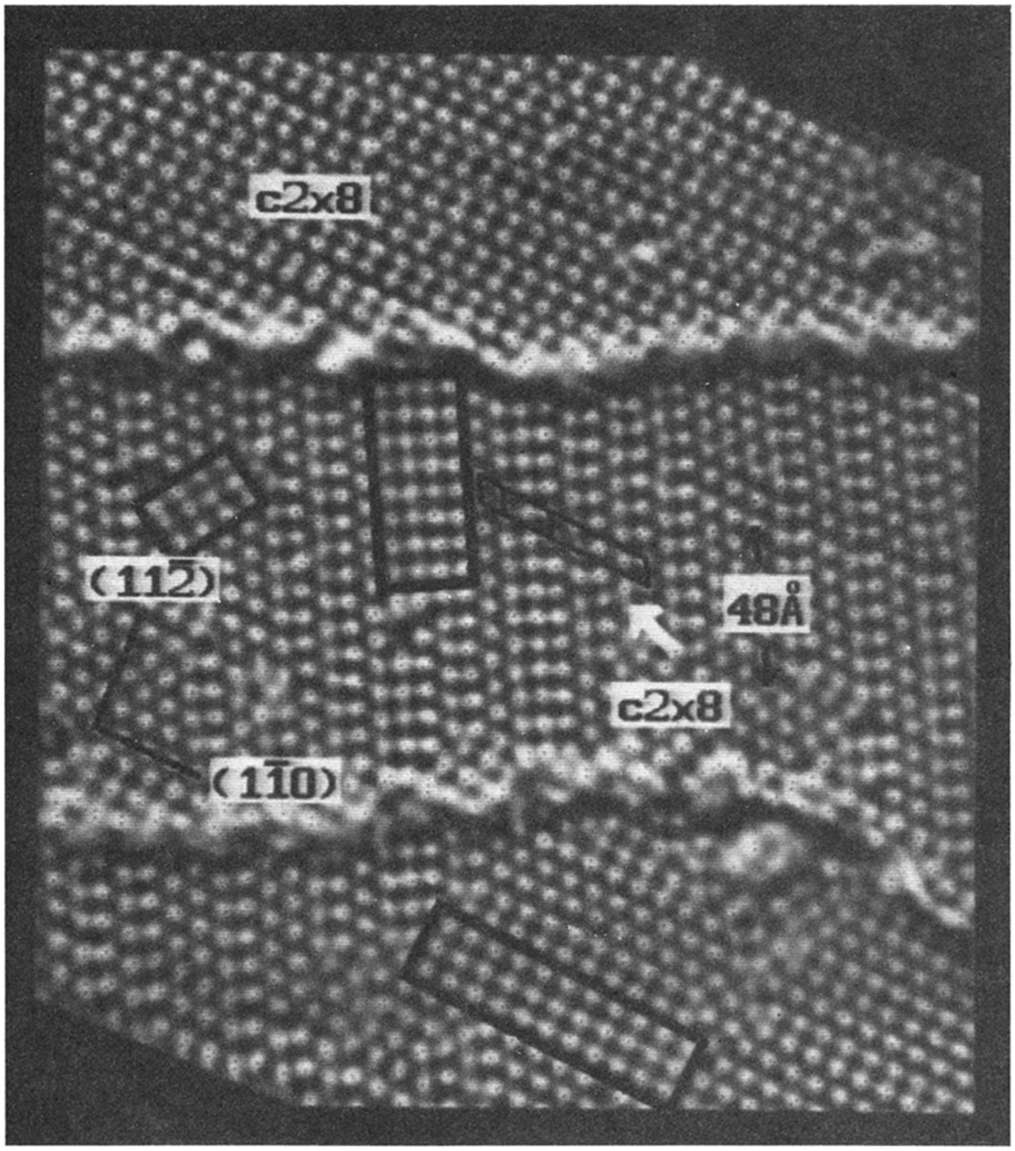

FIG. 1. Tunneling image of the Ge(111) surface. The grey scale rendering is keyed on curvature, reflecting local height, with a dynamic range of ~1 Å. The principal crystallographic directions are indicated, as are local regions of 2×2, $c(4\times2)$, and $c(2\times8)$ symmetry. Two atomic steps are seen running across the image, which is approximately 260 by 300 Å. This image was acquired tunneling into empty sample states at a bias voltage of 1.0 V at a tunneling current of 40 pA.

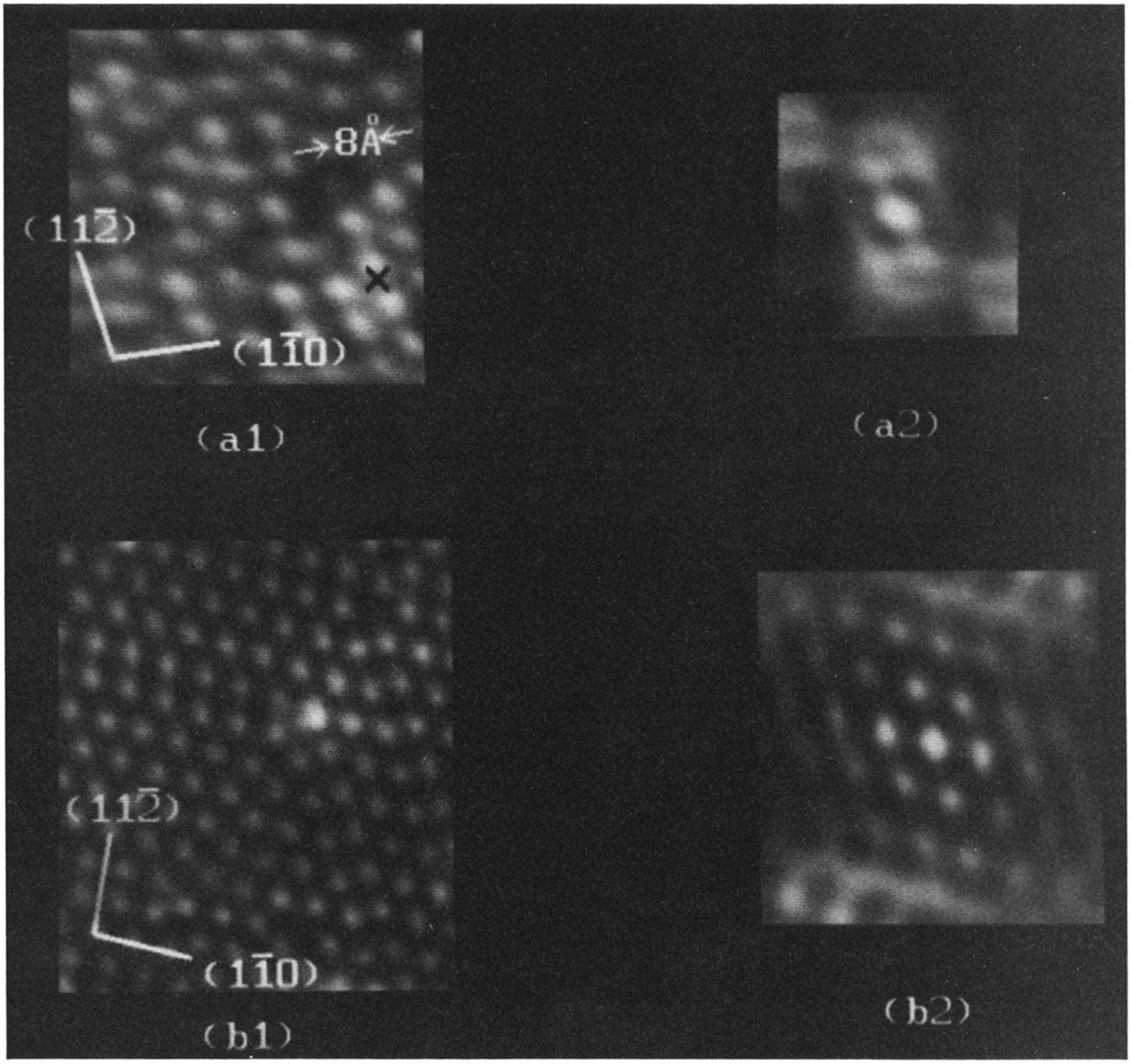

FIG. 10. Tunneling images and their autocorrelations for laser-stabilized Si(111) [(a1) and (a2)], and Ge(111) [(b1) and (b2)]. The crystallographic directions are indicated along with the scale for both images. The *X* denotes a large region of $\sqrt{3}$ symmetry.

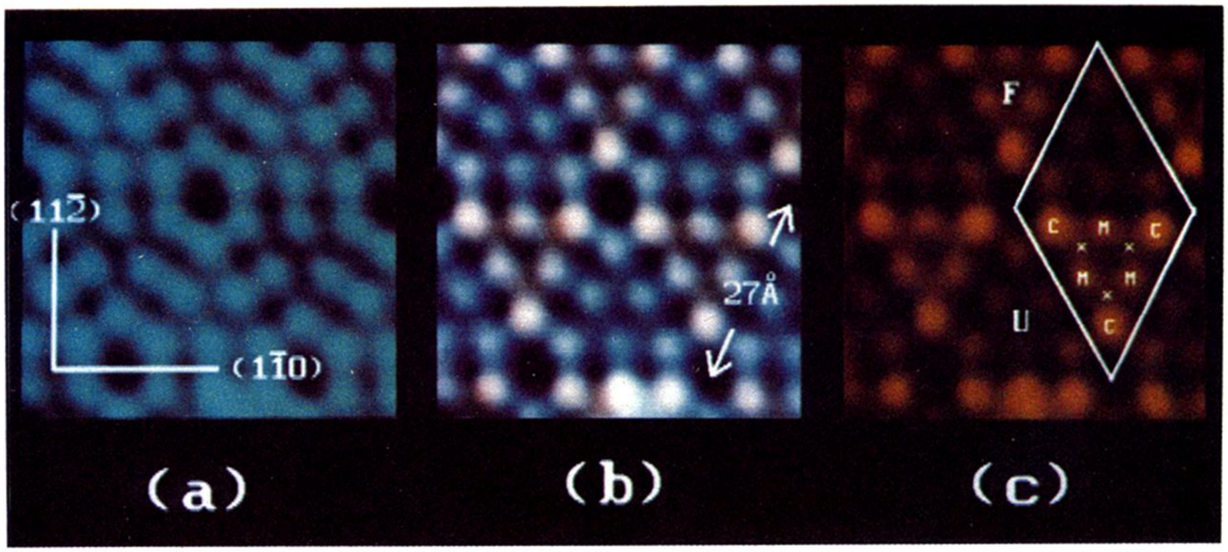

FIG. 2. Tunneling images of Si(111)-(7×7). (a) Unoccupied-state image (blue) taken at +1.0 V. (c) Occupied-state image (orange) taken at −1.0 V. (b) Superposition of the images shown in (a) and (c). The principal crystallographic directions are indicated, along with the image scale. *F* and *U* denote the faulted and unfaulted mesh halves, respectively. *C*, *M*, and *X* denote the positions of corner adatom, middle adatom, and rest-atom dangling bonds, respectively. The color saturation is keyed on height, with a range of 1.0 Å in (a) and 1.2 Å in (c). The demanded tunneling current was 1 nA for both images.

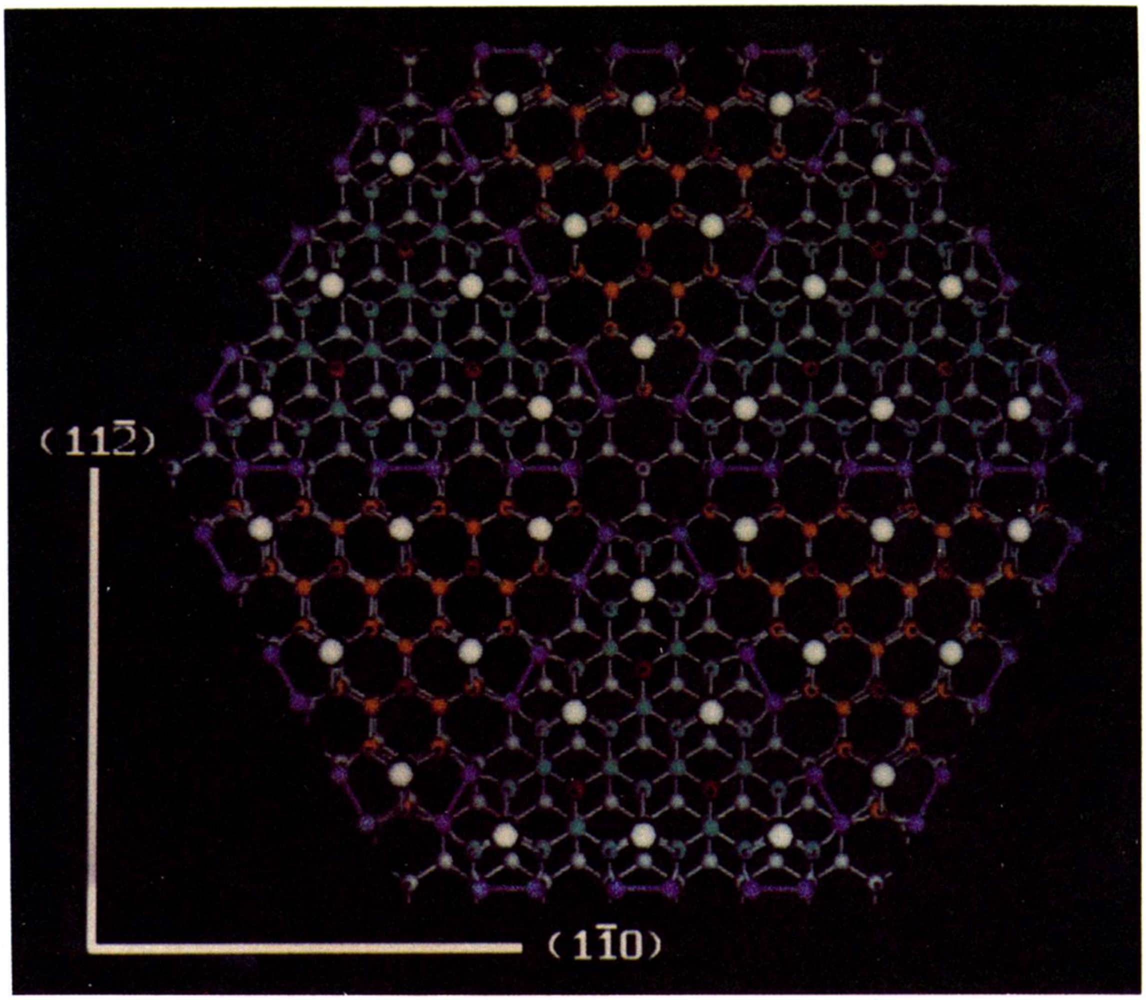

FIG. 3. Model of the dimer-adatom-stacking fault Si(111)-(7×7) surface. The colors for the rest atoms and substrate atoms for the faulted and unfaulted mesh halves are keyed to agree with the tunneling images in Fig. 2. Adatoms are in white, rest-atom dangling bonds in red, unfaulted backbond atoms in blue, faulted backbond atoms in orange, and dimerized domain wall atoms in magenta.

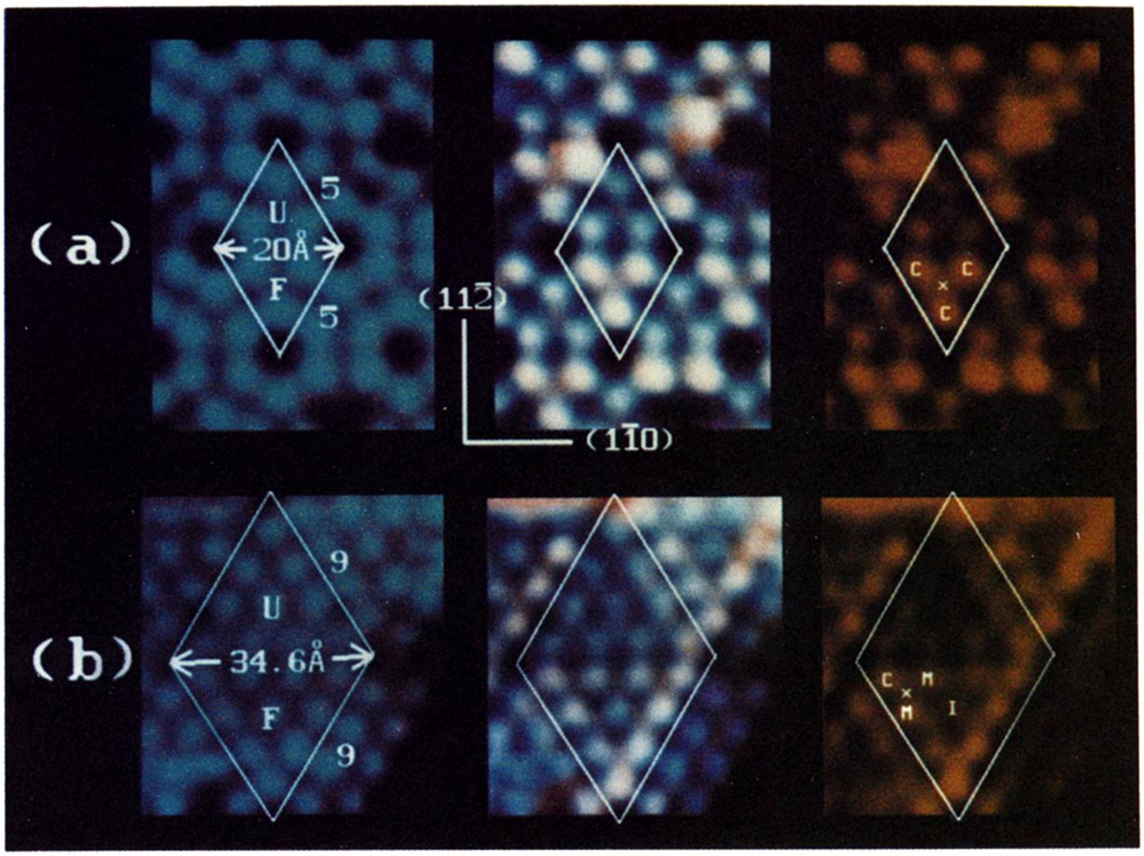

FIG. 4. Dual-polarity tunneling images for (a) Si(111)-(5×5) and (b) Si(111)-(9×9). The blue pictures represent unoccupied-state images while the orange images represent occupied-state images, with their superposition in the center as in Fig. 2. A unit mesh is outlined for the 5×5 and 9×9 with the principal crystallographic directions indicated. The *F* and *U* denote the faulted and unfaulted halves of the unit mesh. In the occupied-state (orange) images, the *C*, *M*, *I*, and *x* denote corner adatom, middle adatom, interior adatom, and rest-atom dangling bonds, respectively. The unoccupied-state image for the 5×5 was acquired at +1.5 V, the occupied-state image at −1.5 V. The 9×9 unoccupied-state image was acquired at +1.5 V and the occupied-state image at −1.7 V. All images were acquired at a demanded tunneling current of 1 nA. The color saturation is keyed on apparent height, with a dynamic range of ∼1 Å.

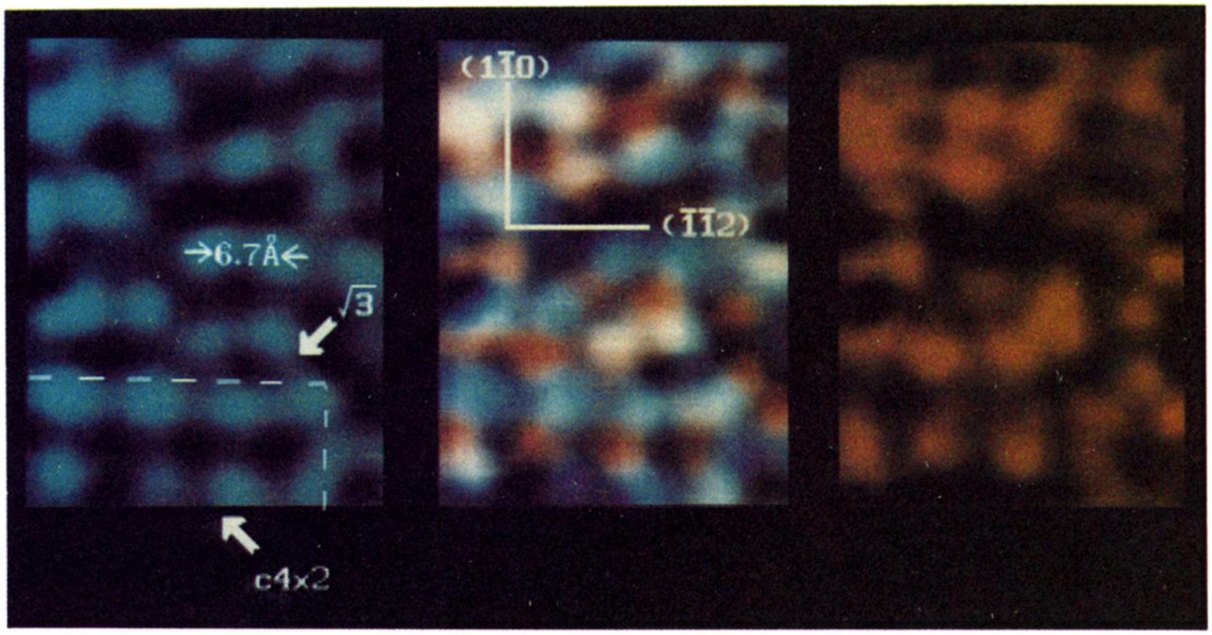

FIG. 5. Dual-polarity tunneling images for laser-stabilized Si(111). (a) Unoccupied-state image acquired at +1.0 V. (c) Occupied-state image acquired at −1.0 V bias. (b) Superposition of (a) and (c). The crystallographic directions and image scale are indicated. The arrow and dashed lines denote small regions of $c(4\times2)$ and $\sqrt{3}$ symmetry. The color saturation is keyed on height, with a range of 1.2 Å in (a) and 0.7 Å in (c). Both images were acquired at a tunneling current of 1 nA.

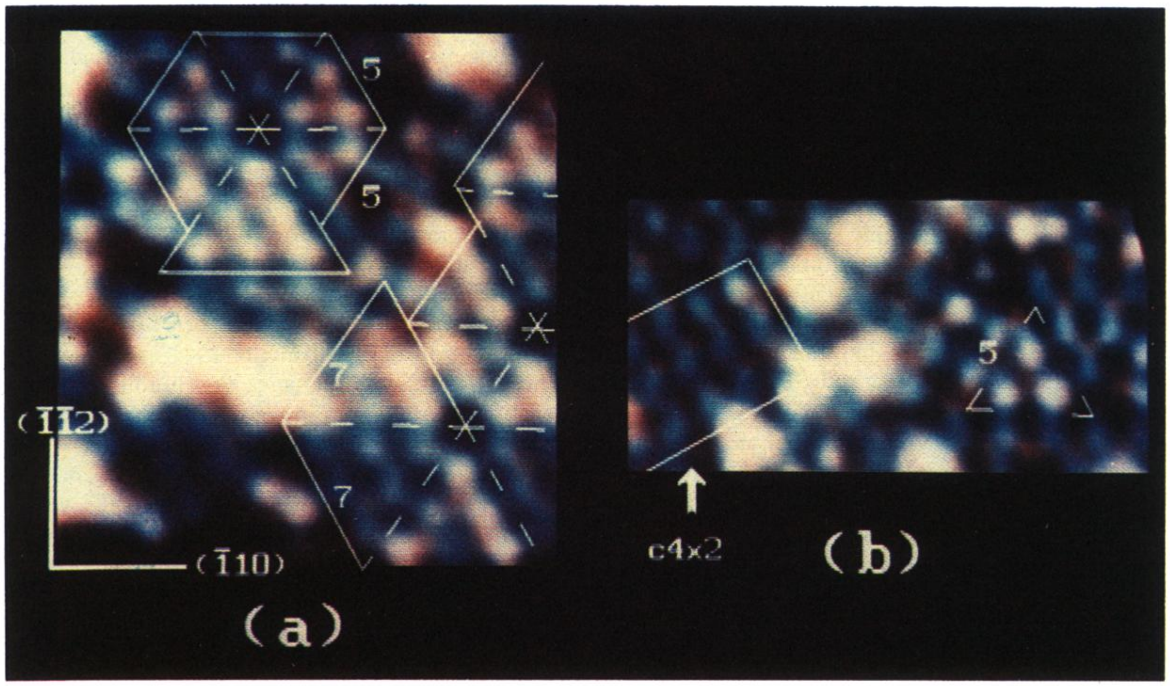

FIG. 7. Superimposed dual-polarity tunneling images for laser-stabilized and partially reannealed Si(111). Blue represents the unoccupied-state image, orange represents the filled-state image, while white indicates both. The solid and dashed lines in (a) denote regions of 5×5 and 7×7 symmetry reconstructed in the DAS fashion. The solid lines in (b) enclose a region of $c(4\times2)$ symmetry while the dashed lines denote a DAS 5×5 mesh. The principal crystallographic directions are indicated. These images were acquired at 1.5 V bias and 1.0 nA tunneling current in both polarities.

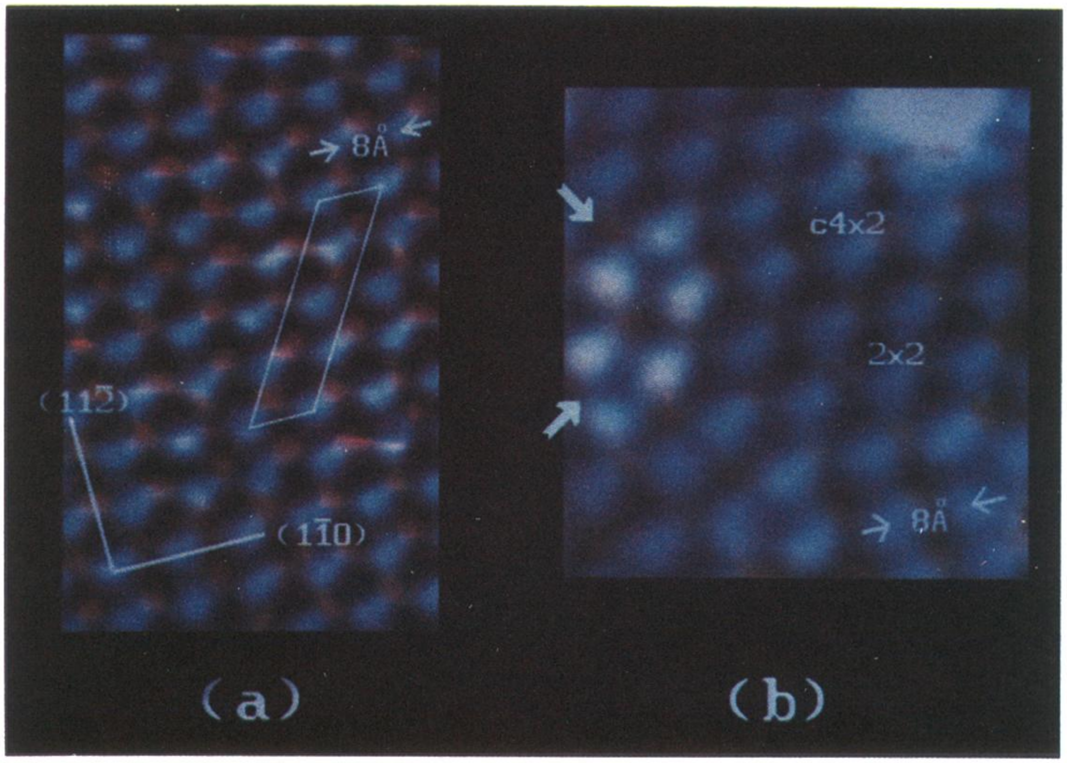

FIG. 8. Superimposed dual-polarity tunneling images for (a) the Ge(111)-$c(2\times8)$ surface, and (b) 2×2, $c(4\times2)$, and $\sqrt{3}\times\sqrt{3}$ domains. Blue represents the unoccupied-state image, orange the occupied-state image, and white both. The principal crystallographic directions are indicated. The solid lines enclose a $c(2\times8)$ unit mesh in (a). The arrows denote a local region of $\sqrt{3}$ symmetry in (b) large enough to show unoccupied-occupied state superposition. Local regions of 2×2 and $c(4\times2)$ symmetry are indicated. The unoccupied-state image was acquired at +2.0 V and the occupied-state image at −2.0 V 1.0 nA demanded tunneling current. The color saturation is keyed on height, with a range of 0.8 Å for the unoccupied-state image and a range of 0.5 Å for the occupied-state image.

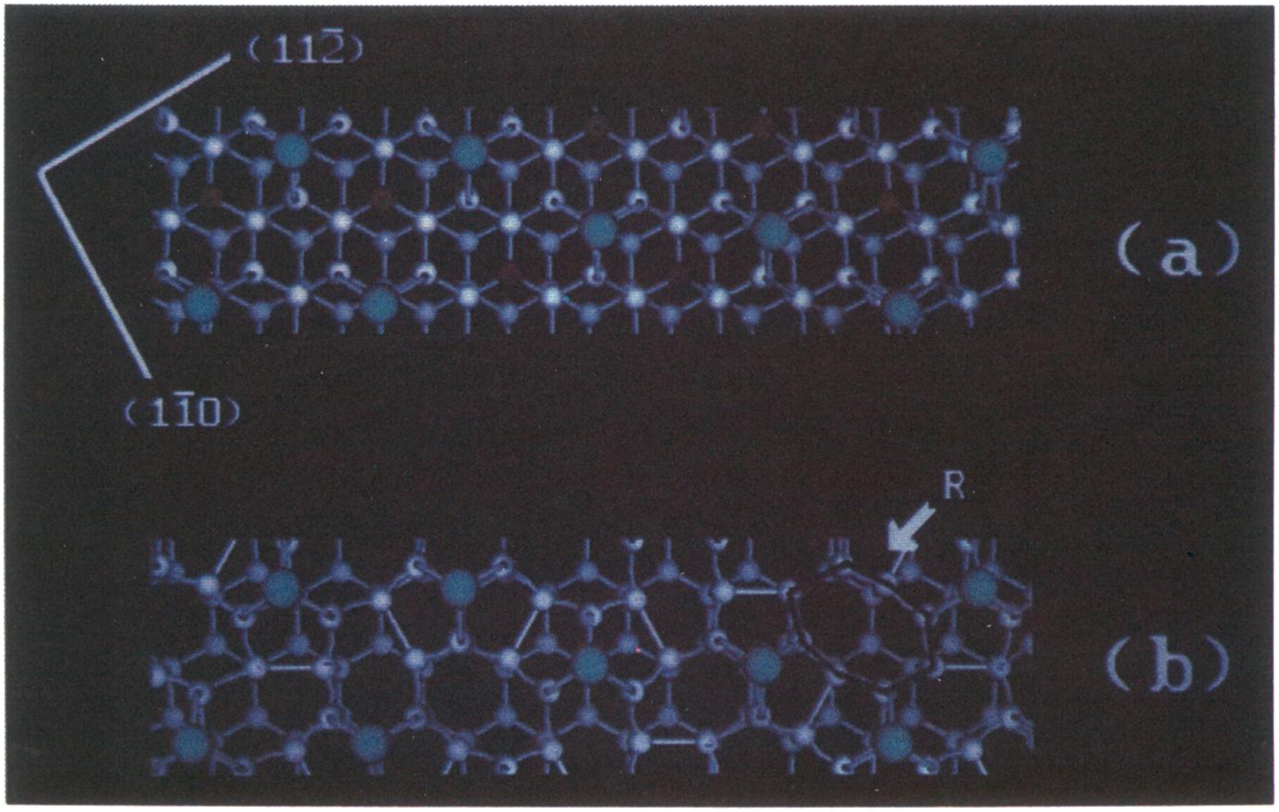

FIG. 9. Ball-and-stick models for the Ge(111)-$c(2\times8)$ surface. (a) Simple adatom phase. (b) Takayanagi dimer-chain adatom phase. Blue denotes adatom and orange denotes rest-atom dangling bonds. The heavy black lines and the *R* in (b) denote an eight-member ring similar to those in the dimer walls in the DAS reconstructions.